MAX PLANCK INSTITUTE
FOR SOLAR SYSTEM RESEARCH

User Guide to
the RAPID Measurements
in the Cluster Science Archive (CSA)

prepared by
Patrick W. Daly and Elena A. Kronberg

Version 7.1

Table of Contents

Reference Documents

RAP-GSE: Daly, P. W. [2004]. Converting from RAPID Coordinates to GSE. *RAPID Report DS–RAP–TN–0019, Issue 1.1*, Max-Planck-Institut für Sonnensystemforschung, Katlenburg-Lindau, Germany. http://caa.esac.esa.int/documents/teams/RAPID/CL_CD_RAP_Convert_to_GSE__20041012_V11.pdf.

RAP-ICD: Daly, P. W., Mühlbachler, S., and Kronberg, E. A. [2025]. Cluster Science Archive: Interface Control Document for RAPID. *Report CAA–RAP–ICD–0001, Issue 9.1*, Max-Planck-Institut für Sonnensystemforschung, Göttingen, Germany. http://caa.esac.esa.int/documents/ICD/CAA_EST_ICD_RAP_v9.1.pdf.

Hapgood, M. A. [1992]. Space Physics Coordinate Transformations: A User Guide. *Planet. Space Sci.*, **40**, 711–717. DOI:10.1016/0032-0633(92)90012-D.

RAP-CR: Kronberg, E. A., Daly, P. W., and Vilenius, E. [2025]. Calibration Report of the RAPID Measurements in the Cluster Science Archive (CSA). *RAPID Report CAA–EST–CR–RAP, Issue 10.1*, Max-Planck-Institut für Sonnensystemforschung, Göttingen, Germany. http://caa.esac.esa.int/documents/CR/CAA_EST_CR_RAP_v101.pdf.

RAP-FOM: [2000]. RAPID Flight Operation User Manual. *Version 3.0*, Max-Planck-Institut für Aeronomie, Katlenburg-Lindau, Germany. http://caa.esac.esa.int/documents/teams/RAPID/CL_CP_RAP_FOP_Manual__20000617_V30.pdf.

Smirnov, A. G., Kronberg, E. A., Daly, P. W., Aseev, N. A., Shprits, Y. Y., and Kellerman, A. C. [2020]. Adiabatic Invariants Calculations for Cluster Mission: A Long-term Product for Radiation Belts Studies. *J. Geophys. Res.*, **125**, e2019JA027576. DOI:10.1029/2019JA027576.

Wilken, B., Axford, W. I., Daly, P., Daglis, I., Güttler, W., Ip, W. H., Korth, A., Kremser, G., Livi, S., Vasyliunas, V. M., Woch, J., Baker, D., Belian, R. D., Blake, J. B., Fennell, J. F., Lyons, L. R., Borg, H., Fritz, T. A., Gliem, F., Rathje, R., Grande, M., Hall, D., Kecskeméty, K., Mckenna-Lawlor, S., Mursula, K., Tanskanen, P., Pu, Z., Sandahl, I., Sarris, E. T., Scholer, M., Schulz, M., Sørass, F., and Ullaland, S. [1997]. RAPID: The Imaging Energetic Particle Spectrometer on Cluster. *Space Science Reviews*, **79**, 399–473. DOI:10.1023/A:1004994202296.

Wilken, B., Daly, P. W., Mall, U., Aarsnes, K., Baker, D. N., Belian, R. D., Blake, J. B., Borg, H., Büchner, J., Carter, M., Fennell, J. F., Friedel, R., Fritz, T. A., Gliem, F., Grande, M., Kecskemety, K., Kettmann, G., Korth, A., Livi, S., McKenna-Lawlor, S., Mursula, K., Nikutowski, B., Perry, C. H., Pu, Z. Y., Roeder, J., Reeves, G. D., Sarris, E. T., Sandahl, I., Søraas, F., Woch, J., and Zong, Q.-G. [2001]. First Results from the RAPID Imaging Energetic Particle Spectrometer on board Cluster. *Ann. Geophys.*, **19**, 1355–1366.

List of Acronyms

BM	Burst Mode, Cluster high telemetry rate
CEF	Cluster Exchange Format (CSA format)
CR	Calibration Report
CSA	Cluster Science Archive
DPU	Digital Processing Unit
EDB	Experiment Data Block
ENA	Energetic Neutral Atoms
GEI	Geocentric Equatorial Inertial coordinate system
GSE	Geocentric Solar Ecliptic coordinate system
ICD	Interface Control Document
IES	Imaging Electron Spectrometer (part of RAPID)
IIMS	Imaging Ion Mass Spectrometer (part of RAPID)

MCP	Multichannel Plate
MPS	Max-Planck-Institut für Sonnensystemforschung, Göttingen, Germany
NM	Nominal Mode, Cluster low telemetry rate
PSD	Phase Space Density
RAPID	Research with Adaptive Particle Imaging Detectors (Cluster Experiment)
SCENIC	Spectroscopic Camera for Electrons, Neutral, and Ion Composition (part of RAPID)
TOF	Time-Of-Flight

1 Introduction

The RAPID experiment (*Research with Adaptive Particle Imaging Detectors*) on board Cluster measures 3-D energetic electron and ion fluxes in the energy range above ~30 keV. Since the raw data delivered by the instrument are of no use without detailed knowledge of their construction, functioning, calibrations, and limitations, it is essential that the RAPID Team process this initial data set into more usable format showing physical parameters in physical units, and make them available to the scientific community. The RAPID team delivers about 50 different data products per spacecraft for each day of observations.

This User's Guide explains how to exploit the CSA RAPID dataset, how to select the right products for various applications, as well as which problems might be encountered, and what the user must watch out for.

It is intended to be concise and uncomplicated; therefore only the main products will be discussed here. A complete description of the RAPID CSA data products is given in the RAPID Interface Control Document [RAP-ICD] and the data quality issues are described in the RAPID Calibration Report [RAP-CR].

- For emphasis, important caveats are bulleted and placed inside a gray-shaded box.

1.1 Major Failures

The major failures that have occurred so far are summarized here for quick reference.

- The central ion detector head failed early in the Mission on all spacecraft (Section 3.3.2).
- On SC4, only ion head 1 was functioning from from 2003 to 2006 (Section 4.2).
- On SC1, the high voltages for the time-of-flight system failed on March 16, 2007, so no ion measurements are possible after this date (Section 4.2.1).
- On SC3 the high voltages for the time-of-flight system failed on December 1, 2009, so no ion measurements are possible after this date (Section 4.2.1).
- For all spacecraft, the central electron detectors have started to degrade beginning in 2007 (Section 4.1.1).
- On SC2, the electrons failed on March 26, 2015; however a partial recovery of 3 out of 9 detectors is possible as of June 12, 2015 (Section 4.1.1).

1.2 End of Mission

The operation phase of the Cluster Mission ends on September 30, 2024. However, there are some intermediate steps that apply to RAPID.

SC1: RAPID was turned off permanently on September 19, 2023, as a power-saving measure for the other instruments. This was at the start of a long-eclipse season.

SC2: all instruments, including RAPID, were turned off on February 1, 2024, at the start of the final short-eclipse season, and were not powered up afterwards, pending the re-entry of this spacecraft on September 8, 2024.

SC3, SC4: all instruments are shut off on September 30, 2024; end of all data-taking for Cluster.

Table 1: The standardized RAPID energy channels
Lower thresholds, all units keV

Channel	Hydrogen	Helium	CNO	Electrons	
				BM	NM
1	27.7–64.4[a]	(29.9)[b]	(83.8)[c]	39.2[d]	39.2[d]
2	75.3	137.8	274.4	50.5	50.5
3	92.2	172.3	414.	68.1	68.1
4	159.7	235.1	498.	94.5	94.5
5	374.	351.	638.	127.5	127.5
6	962.	737.	948.	175.9	244.1
7	1885.	1689.	1414.	244.1	—
8	—[e]	—[e]	2539.	336.5	—
Upper	4007.	3799.	4046.	406.5	406.5

[a] Energy gap between hydrogen 1 & 2

[b] Helium channel 1 contains hydrogen, suppressed

[c] CNO channel 1 contaminated, suppressed

[d] Revised value, was previously 37.3 keV and 41.2 keV, see Sec. 7 in RAP-CR

[e] 8th channel not accessible for hydrogen and helium

2 Instrument Description

The RAPID experiment is described in *Wilken et al.* [1997] as well as in the Flight Operational Manual [RAP-FOM]. The first results are presented in *Wilken et al.* [2001].

The RAPID instrument uses two different and independent detector systems for the detection of nuclei and electrons: The **I**maging **I**on **M**ass **S**pectrometer (IIMS) and the **I**maging **E**lectron **S**pectrometer (IES).

2.1 The IES Instrument

One of the three IES detector heads is shown in the left side of Figure 1. Each functions as a pin-hole camera, with 3 microstrip detectors to locate the incoming particles to within 20°. Not shown is a foil between the pin-hole aperture and detectors that removes any ions up to 350 keV.

A single head covers an acceptance angle of 60° in all; a total of three heads span the entire range of 180° with 9 "pixels" (middle of Figure 2) in one half-plane. During one spacecraft spin (∼4 s), this plane rotates through 360°, during which time, 16 measurements are made; one speaks of 16 spin sectors which are synchronized to the sun (right side of Figure 2). A 3-D distribution thus consists of 9 polar × 16 azimuth directions.

The 3rd dimension, energy, is determined by the charge deposited in the detector by the absorbed electron, which is proportional to that energy (minus a constant). IES employs an integration method for this: that is, it accummulates the total charge deposited by all particles during a selected integration time; the total charge (corresponding to the total energy) is then swept out and measured during a fixed read-out time, which constitutes a dead-time. Thus the total number of samples per second is always the same for a given integration time. The analog signal is digitized to a bin number between 0 and 255, at 2.2 keV per bin. The number of such counts in each bin can be plotted as a histogram as in Figure 3. The majority of these samples do not correspond to any real particle, but contribute instead to the *pedestal*, the location of zero energy. The pedestal arises because the detectors are slowly charged during the integration time by background currents. The actual 6–8 science channels are defined onboard in terms of the 256 bin numbers, relative to the expected location of the pedestal, such that they correspond to the values listed in Table 1.

Since the pedestal location and width vary over time, it is necessary to revise the definitions periodically and to
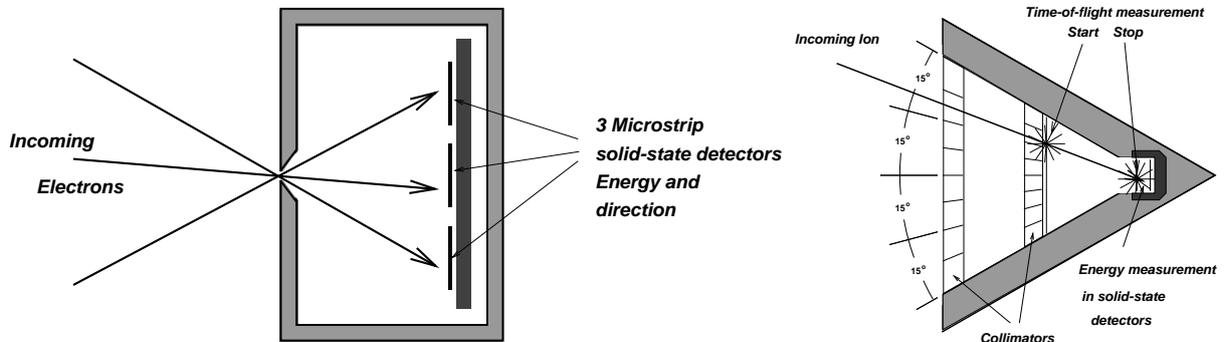
Figure 1: Left: One of the three IES heads, containing three solid state detectors to determine the direction of the incoming detected electron to within 20°. Right: One of the three SCENIC heads making up the IIMS part of RAPID. Shown is an incoming ion that triggers a start signal at a foil, which also serves to determine the fine direction, and a stop signal when it enters the solid state detector, where its energy is measured. The stop and start signals are detected by multichannel plates (MCPs), not shown.
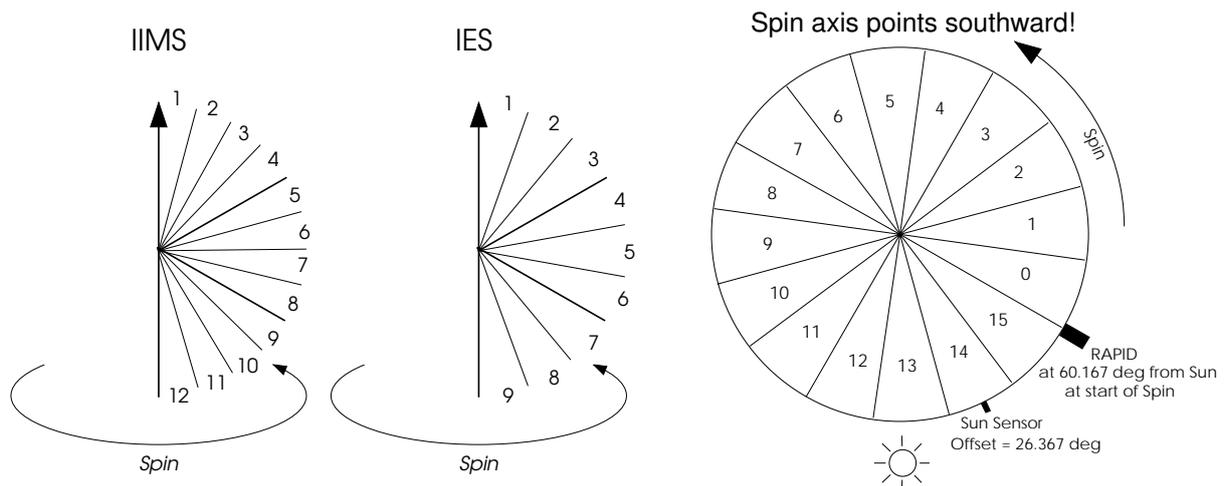
Figure 2: The IIMS and IES polar segments relative to the spin axis (left and center) and the RAPID sectorization relative to the sun (right). *Note that the spin axis actually points towards the $-Z$ GSE axis (southward).*
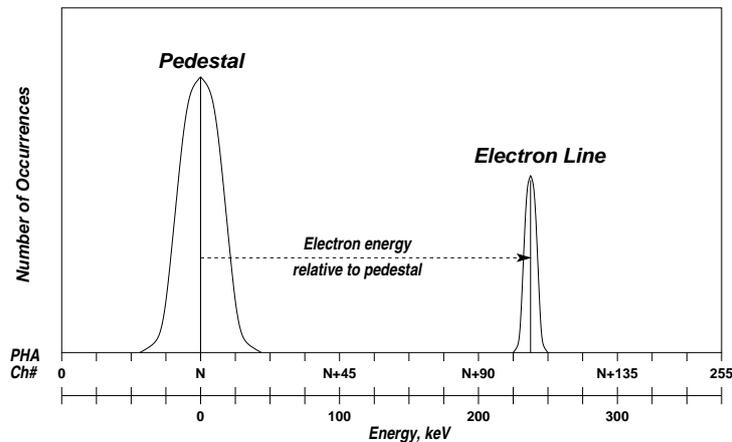
Figure 3: An idealized histogram plot for IES data. The number of measurements per second is constant, depending on integration time. The majority of measurements are empty, contain just a background charge but no electrons, and they form the *pedestal* (large peak at left). True electrons deposit an additional charge, so that a monoenergetic beam could create the peak at the right. The center of the pedestal thus corresponds to the zero of energy.

upload new values to the spacecraft. Methods do exist to try to monitor the instantaneous pedestal location (it can depend on count rate) and to correct the processed electrons fluxes on the ground (Section 4.3).

Note that since each sample measures the total charge deposited during the integration time, it is necessary to keep this time short enough to avoid multiple hits (i.e. *pile-up*), yet long enough to reduce the total dead-time. An *auto-switching* algorithm is applied to automatically select the optimal integration time (see Section 3.2).

2.2   The IIMS Instrument

A single ion SCENIC detector head is illustrated on the right side of Figure 1; there are three ion heads in total. The entering particle first traverses collimating plates, penetrates a thin foil that emits electrons to generate a start signal, and then strikes the solid state detector, where electrons emitted at the surface produce a stop signal. The particle energy is deposited in the detector and is recorded.

The start and stop signals are generated by electrons emitted from the initial thin foil and the surface of the detector respectively; a grid at a negative potential (not shown in the figure) reflects these electrons into the start and stop MCPs, positioned on opposite sides of the unit. Each of the start and stop signals has its own efficiency factor, which depends on the MCP characteristics, such as applied high voltage and age.

The opening angle for a single ion detector is also 60°, but unlike for the electrons, the subdivision into four 15° slots is done by determining the location of the signal at the start MCP. The efficiency of this directional determination depends not only on that of the start signal itself, but also on the probability of obtaining an unambiguous result.

The start and stop signals are used to measure the time-of-flight (TOF) over the 32 mm separation. This time together with the measured energy locate the event within the energy-TOF space of Figure 4 which then determines the species and energy channel. The number of events in each of the species-channel bins in Figure 4 is read out and then zeroed after each sector (1/16 spin).

Only the hydrogen, helium, and carbon-nitrogen-oxygen (CNO) data are delivered by RAPID as part of the regular products; the silicon-iron channels are also available but only in the direct events product (see RAP-ICD).

There is a special mode for **energetic neutral atoms** (ENA), in which a cross voltage of up to 10 kV is applied just behind the entrance aperture, to sweep out ions of up to ∼ 150 keV. In this mode, only neutral atoms are detected
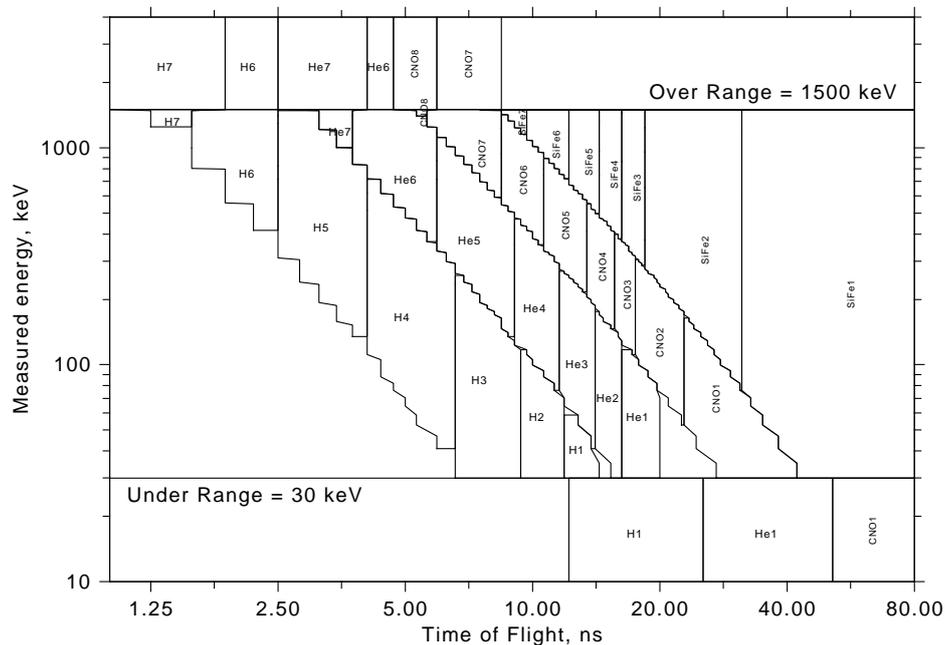
Figure 4: The RAPID ion classification system. Every ion "event" occupies a point in the $256{\times}256$ energy-TOF space, which is divided into areas for different ion species and up to 8 energy channels. For events of (internal) energy $< 30\,\text{keV}$, no energy signal is produced. In this "underrange" region, species determination is done solely with TOF and the fact that the energy is below this threshold.

and processed. This mode has only been used on SC4 in the solar wind during the first two years of operation, as listed in Appendix D of RAP-CR. There are separate products for the omnidirectional and 3-D flux data, to distinguish them from the corresponding ion fluxes (Section 5.1.3).

2.3   Spin Sectorization

For both IIMS and IES, the azimuthal distribution of particle fluxes is obtained by sorting the counts into 16 sectors during one rotation of the spacecraft (right side of Figure 2).

The spin phase relationship between the sun sensor pulse and the start of sector 0 (the start of a new spin) is fixed so that the RAPID detectors are looking into the direction of the sun at sector 13.326, or about one third into sector 13. (This relationship has been set in agreement with the other experiments so that all start a new spin simultaneously.)

Note: For the IES heads 1 and 3, there are really only 8 azimuthal sectors in the raw data. In order to simplify the dataset for the users, the processed data are put into regular rectangular matrices of $9{\times}16$. This is done by splitting each of the 8 sectors into two and by placing half the counts into each sector half. Thus for the polar directions 1–3 and 7–9, although 16 sectors exist formally, the fluxes in each pair (0,1), (2,3) ... (14,15) are identical.

3   Instrument Operations

3.1   Telemetry modes

The Experimental Data Block (EDB) contains the compressed science data produced by the Digital Processing Unit (DPU). One EDB is generated per spin ($\sim$4 s). The data structure varies with the telemetry mode. The

RAPID telemetry formats are:

NM: Nominal mode is active most of the operation time of the instrument with 1024.8 bits/second.

BM: Burst mode allows four times more data downlinked than NM. The principal difference between BM and NM is a higher sampling rate for the 3-D ions and enhanced 3-D electron products.

BM3: This mode, lasting ∼5 minutes once a day, is intended to read out scratch memories of some instruments. For RAPID, BM3 simply forms a data gap during this time.

NM3: Nominal mode 3 is a special mode on SC2 only, used between July 2003 and April 2004; in this mode, RAPID "borrows" extra bandwidth from the non-functioning CIS instrument so that the data are in BM format even though the spacecraft telemetry mode is NM.

It was also used from March 29 to April 3, 2011, on SC2 and SC3 (where CIS had subsequently failed) as part of a special Guest Investigator program.

The times for NM3 are listed in Appendix F of this document.

Note: NM3 was an attempt to improve the angular resolution of the electron 2-D data in NM. It became unnecessary after May 2004 when the new L3DD product became available on all 4 spacecraft (see Section 5.1.1, page 18 and Table 2).

The telemetry modes can be checked in the RAPID 6-hour *Summary Plots,* described in Section 5.6, in the 6th panel of Figure 11—*IIMS Modes, TM.* These are available from CSA (as *Quicklook Plots*), or directly from MPS at `http://www2.mps.mpg.de/cgi/rapid/sumplot.cgi`.

Alternatively the telemetry mode information is also contained in the DSETTINGS product (see Section 5.3).

3.2   Operations on IES (electrons)

As described in Section 2.1, the RAPID detectors work in an integration manner: measurements are constantly being made over a certain *integration time*, and the results read out over the next $48\,\mu$s (the *dead time* which is fixed for all integration times). The integration time can be set to 2, 5, 15, and $50\,\mu$s. The *duty cycle* (fraction of time the detectors are open to detection) thus ranges between 4% (at $2\,\mu$s) and 50% (at $50\,\mu$s).

During each measurement, there can be zero, one, or even more electrons entering the detector, but only the summed energy is determined. Thus to avoid multiple electrons entering during a single measurement (*pile-up*), the integration time should be kept low, which reduces the duty cycle considerably. The integration time is therefore automatically optimized by means of an *auto-switching* algorithm that depends on the count rate (low rate, long integration and vice versa).

Caveats:

- There can be apparent jumps in the flux values when the integration times switches too late, i.e. as the pile-up effects are suddenly removed. This problem is most serious before January 25, 2002, when the automatic switching was occurring too late. After this date the timing of the auto-switching was improved by modifying the parameters involved. The problem was thus reduced, but not entirely eliminated. Further improvement was made after November 6, 2013 when the parameters were again adjusted for faster switching.

  Corrections for this are not possible; the user must be careful with such jumps. An example of switches of the integration time and its effects can be seen in Figure 5.

- From January 18 to February 20, 2004, the automatic switching on SC4 was turned off by mistake; the integration time remained fixed at $50\,\mu$s (Figure 6).
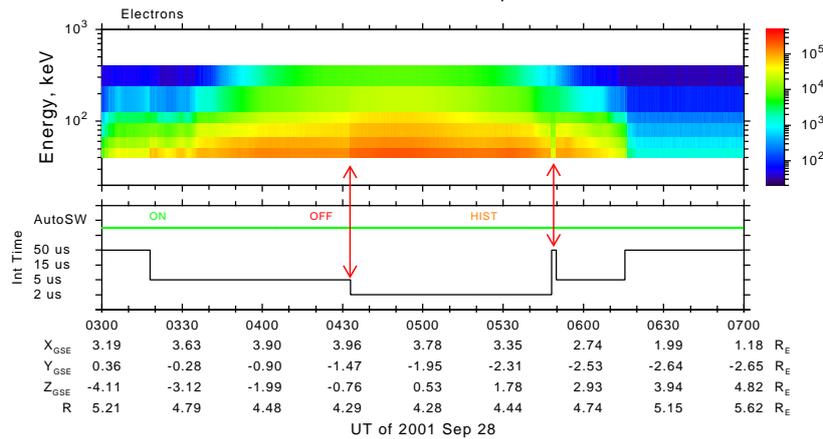
Figure 5: Demonstration of how changes in the IES integration times can produce erroneous changes in the electron fluxes if the automatic switching occurs too late (times are denoted by red arrows). For example at ~04:32 integration time (second from the top panel) switches from $5\,\mu s$ to $2\,\mu s$ and produces the sudden sharp change in the electron intensity. Another example one can see at ~05:49, when integration time was erroneously switched from $2\,\mu s$ to $50\,\mu s$ and than back to $5\,\mu s$ producing a sharp intensity drop for the time of the too-long integration time.
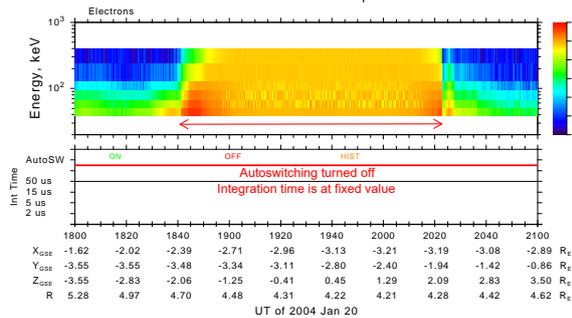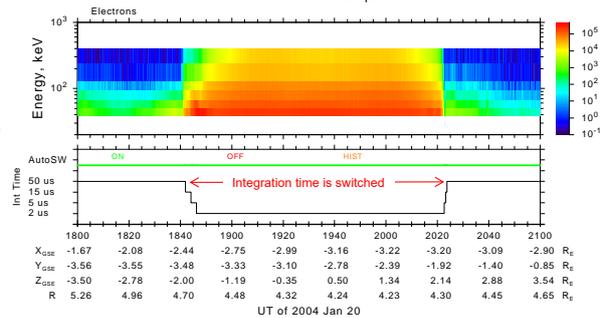
Figure 6: Left: An illustration of what can happen when the integration time fails to switch. As the intensities increase, the count rates in the lowest channels are too low, since multiple low-energy events count as a single high-energy one. Right: For a comparison the same time period and the same region measured by another Cluster spacecraft where the auto-switching was working properly.

The information on integration time switches can be found in the *Quicklook Plots,* by selecting plot `C*_CG_RAP_SUMPLOT_D`, 5th panel — *Int Time*. This information is also available in the *"Status"* product `DSETTINGS` (Section 5.3).

For example, the `DSETTINGS` entries corresponding to the data shown in Figure 5 are:

```
2001-09-28T04:05:46.280Z/2001-09-28T04:32:54.060Z, 0, 1, 1, 0, 155, 111, 0, 0, 1, 5 , 1 $
2001-09-28T04:32:54.060Z/2001-09-28T05:40:43.516Z, 0, 1, 1, 0, 155, 111, 0, 0, 1, 2 , 1 $
.  .  .  .
2001-09-28T05:48:04.541Z/2001-09-28T05:49:48.783Z, 0, 1, 4, 0, 3373, 3322, 0, 0, 1, 50 , 1 $
.  .  .  .
2001-09-28T05:49:48.783Z/2001-09-28T05:50:48.923Z, 0, 1, 4, 0, 3373, 3322, 0, 0, 1, 5 , 1 $
```

The integration time is the second last item in each line, here shown in yellow. Ones sees that it changes from 5 to $2\,\mu$s at 04:32:54, then to 50 μs at 05:48:04 and then to 5 μs at 05:49:48. (The entries involving other parameters have been removed here.)

3.3 Operations on IIMS (ions)

3.3.1 IIMS instrument modes

In the usual *serial* mode, each ion head accumulates for a fixed 60 ms within each of the 16 azimuthal sectors, one after the other. This means the duty cycle depends on spin rate. For example, for a nominal 4 s spin, each of the 16 sectors requires 250 ms, so each head accumulates for only 24% of the time available (60 ms out of 250 ms). During the remaining dead time, the counts from the previous sector are processed and other housekeeping tasks are performed.

There is also a *parallel* mode that was used occasionally in the solar wind early in the mission; in this mode, all three heads accumulate simultaneously for 180 ms per sector.

In the first few months of the mission, before the main patch was uploaded, the accumulation times were 65 and 195 ms for serial and parallel mode, respectively.

The IIMS instrument modes can be checked on the *Quicklook Plots*, plot `C*_CG_RAP_SUMPLOT_D` in the 6th panel (Figure 11)—*IIMS Modes, A*. This information is also available in the *"Status"* product `DSETTINGS` (Section 5.3).

3.3.2 Damage of the central ion head

- The central ion head on all 4 spacecraft deteriorated within the first months of the mission; most likely sunlight saturated the time-of-flight system. The result is that ion distributions are not available within 30° of the ecliptic plane. This is often referred to as the "donut" effect (hole in the middle). For information on how this caveat affects the 3-D distribution see Figure 7. For the omnidirectional flux products the "donut" effect is taken into account.

4 Measurement Calibration and Processing procedures

Before raw data become scientifically valuable they need to go through various treatment procedures and become reprocessed. Imperfection of some corrections lead to caveats which the user should be aware of.

4.1 Electrons

- **Spectra correction**

Since the pedestal position (see Section 2.1) moves with time (aging), temperature, and even raw count rate, its position is constantly monitored and corrected for in the data. A consequence of this is that the different electron detector strips effectively measure different energies. Efforts are made to correct for this, as described in Section 4.3. However, the corrections are not always perfect and the user should be aware of this.

- **Pedestal noise correction on SC4**

  Pedestal contamination affects the electron omnidirectional distribution. To correct for this, we remove the noisy strips from both the omnidirectional and 3-D data. Correction, as always, is made for the fluxes only, never for the raw count rates. For more details and examples see Section 5.1.3 in RAP-CR.

- **Solar noise correction on SC3**

  Sunlight enters the IES head 1 on SC3 and produces noise in the data. This solar noise is very strongly dependent on solar aspect angle (SAA). A correction is made to both 3-D and omnidirectional flux data. For more details about this correction and examples see Section 5.1.4 in RAP-CR.

- **Inter-spacecraft cross-calibrations**

  Large differences between the electron detectors on different spacecraft are not expected and were initially not compensated for. However, during the analysis for the long-term degradation (see below), some differences were indeed found in the data for the early years. These are considered to be intrinsic, i.e. time constant; their correction factors are now included as part of the overall decay corrections.

4.1.1 Other issues with electrons

Over the course of time, certain problems have arisen regarding the IES instrument, which are covered in detail in the Calibration Report [RAP-CR]. We summarize them here.

- Starting in about 2006, there is an increasing degradation of the IES detectors pointing closest to the spin plane. Several sets of correction factors have been generated to compensate for this, as described in Section 9 of RAP-CR. The latest set, version 15.5, has been used to reprocess all the electron fluxes in early 2021.

  At the same time, corrections for the time-independent differences between the detectors (see above) were also included in this set.

- On March 26, 2015, there was a failure of the IES instrument on SC2, but the 3 detectors 7–9 could be partially recovered, starting June 12, 2015. However, the recovered data are really only good for establishing the presence and timing of electron events. Details are to be found in Section 10 of RAP-CR.

4.2 Ions

- **Time-varying detector efficiencies**

  The start and stop signals are generated by MCPs, whose performances change considerably over time. Thus the overall response, including the TOF efficiency, is monitored continuously and the calibration files are regularly updated. The user must realize that since these parameters are based on long-term averages (over weeks or months) there can be deviations on any particular day. See more details and diagnostics in RAP-CR.

- **SC4 has only one head for 2003–2006**

  Starting on June 21, 2003 at 17:11, the ions on SC4 developed a DPU problem that resulted in only head 1 functioning. All efforts to fix it with repatching the DPU failed. In was not until May 09, 2006 when the unit spontaneously rebooted that the problem vanished. (Reboots cannot be forced, but with age, spontaneous reboots become more frequent.)

  This problem has also arisen on SC3, Jan 28 to Mar 18, 2008, on SC2, Aug 14 to Sep 12, 2011, and on SC4 again Aug 14 to Sep 14, 2011. In these cases, the problem was recognized and a reboot was forced by switching the unit off and on.

  These are all included in the list of events in Appendix G.

- **Inter-spacecraft and inter-head cross-calibrations**

  Efforts are made to cross-calibrate the ion detector performances over the 4 spacecraft and all the functioning heads, by normalizing them such that they all yield the same value for the flux averaged over a long time of days or weeks (see RAP-CR). The user must realize that these inter-spacecraft/inter-head cross-calibrations are therefore only approximate and could deviate on any particular day. This could lead, for example, to an apparent asymmetry between ion head 1 and 3.

- **First energy channel (He, CNO)**

  These channels are included in raw count rates but they are replaced with fill values in particle flux datasets. The lower part of Figure 4 shows the "underrange" region, where no energy signal is received ($<30\,\mathrm{keV}$); ion classification is done solely on TOF information and the fact that the energy is so low. These events contribute to energy channel 1. The species determination is not accurate: low energy hydrogen ions can enter and dominate first channels of helium and CNO (which are therefore suppressed). For more detail, see RAP-CR.

- **Accumulation problem for the 3-D ions, SC1, SC3, SC4 in NM**

  There is a bug in the onboard programming that causes the 3-D ions in different sectors to be accumulated asynchronously, i.e. at different times and out of order. A presentation of this bug is shown in Figure 7. Therefore users using the standard (merged) ion 3-D distributions, should be aware that spurious effects due to time-aliasing could arise, as illustrated in Figure 7. In suspicious cases it is advised to check the expanded ion 3-D distributions which show the partial distributions in the proper time sequence.

  This bug affects only the ion data in nominal mode, and only on spacecraft 1, 3, 4.

4.2.1 Failures of the ion instrument

SC1: the high voltages on the MCPs failed on March 16, 2007, so that no ion data are available on this spacecraft after this date.

SC3: the high voltages on the MCPs failed on December 1, 2009, so that no ion data are available on this spacecraft after this date.

4.3 Standardized Energy Channels

A uniform set of energy channel definitions is essential for any physical analysis of the data. Hence, the variations in the spectra among the sensors are corrected to bring them effectively to such a standardized set. The correction is applied to the each ion and electron sector. The "official" values now used for the CSA products are listed in Table 1.
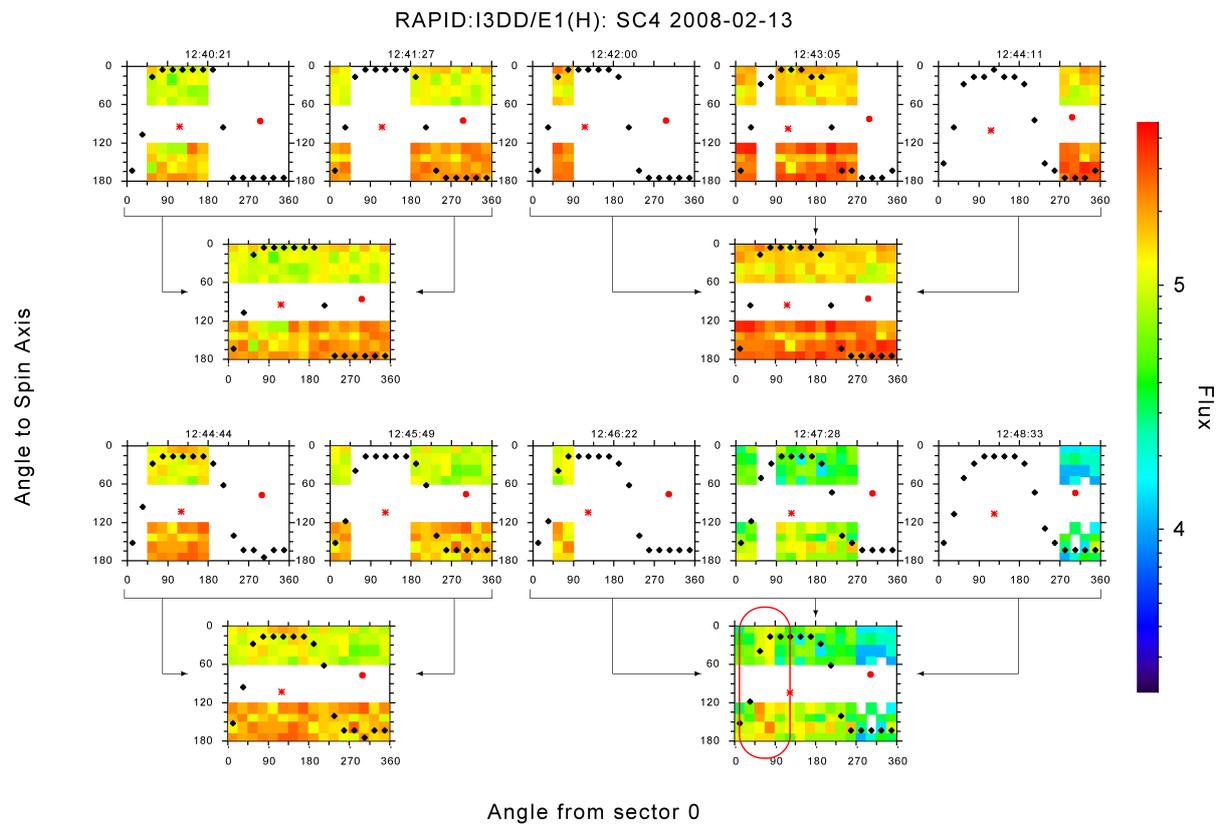
Figure 7: Example of the 3-D ion timing problem. Rows 1 and 3 show the partial distributions, the dataset called as the ion 3-D distribution (expanded) at the CSA, while rows 2 and 4 are the merged full distributions (the ion 3-D distributions (standard) at the CSA). That is, the boxes in rows 2 and 4 are merged versions of the 2 or 3 boxes above them, as shown by the arrows. The red oval at the lower right indicates an apparent anisotropy in the merged data that is really a result of time-aliasing, i.e., the enhanced intensities were actually measured earlier.
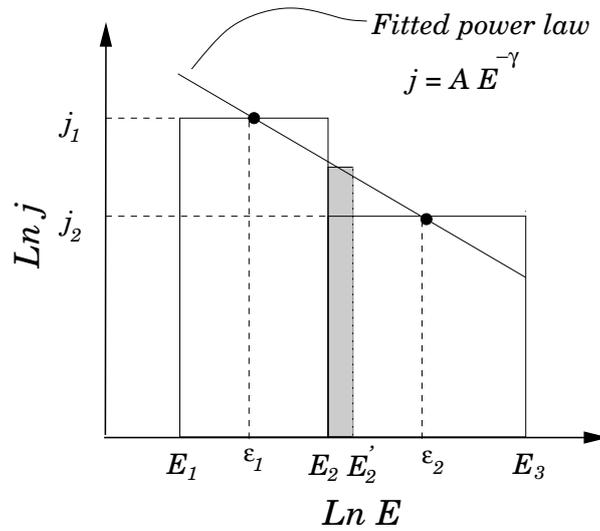
Figure 8: Shifting the energy threshold between two channels: the differential flux in two channels is fitted to a power law, that fit is integrated over the energy shift $E_2' - E_2$ (shaded area), and the result moved from one channel to the other.

The algorithm used for this correction is to fit the data between adjacent channels to a power law which is then integrated over the energy shift region, with the resulting flux subtracted from the one and added to the other channel, as shown in Figure 8.

For the electrons, there is a further adjustment to be made: because the pedestal that defines the energy origin can move in a way that depends on count rate, its location is monitored by some additional diagnostic channels. The spectral shift introduced by this effect can be deduced and then also corrected for as part of the energy channel standardization.

Note that the spectral correction is applied only to flux data, not to the raw count rates since they are to remain as original raw data.

4.4 Phase Space Density Conversion

Conversion factors between differential flux and phase space density are listed in Appendix C.

5 Key Science Measurements and Datasets

5.1 Particle Distributions

The key science measurements for the RAPID instrument are particle distributions in the following units:

Raw Count Rate These are raw data in units of (1/s) with no corrections, calibrations, or suppressions whatsoever; only the *accumulation time* is employed to convert from counts to rates. This accumulation time is well-defined but not trivial to determine, hence it is included as a record-varying parameter in every count-rate dataset. The original number of counts can thus be reconstructed if wanted. The dataset names of the raw data products have an ending suffix ⎯R (see Appendix A for a complete list of datasets).

Number Flux Processed data in units of *differential particle flux*, $1/(cm^2 \, sr \, s \, keV)$. See RAP-ICD for more details.

Standard Deviation For both fluxes and raw count rates, the *standard deviation* is also included in each record, in the same format and array size as the data. This is obtained from both the Poisson statistical error of the

counts plus a factor for the data compression uncertainty; the former normally dominates. See Appendix C in RAP-CR for more details.

For measured zero flux, the standard deviation is also set to zero, although it should really be that for a single count, to express the uncertainty level. However, such a procedure would lead to errors when summing over longer times. Recall that errors are combined by summing the variance, i.e. the sum of the squares of the standard deviations.

Time Tag The record time tag refers to the middle of the record interval; the time-half-interval for each record is also given.

Note that the record interval and the accumulation time are two separate things: data are accumulated over a certain interval but not necessarily for 100% of that time.

5.1.1 Electrons

The electron distributions as delivered directly by IES exhibit some important differences between the nominal telemetry mode (NM, low bit rate) and burst mode (BM, high bit rate), see Section 3.1. All the electron products have a time resolution of one spin, i.e. ~4 s.

Here we list only the datasets in particle flux. The datasets in raw count rates have an additional suffix _R in their names as indicated by the ∗ in the names below. They can be downloaded as well but their use is advised only for experts as these datasets are neither calibrated nor corrected.

Omnidirectional: Omnidirectional electron fluxes are created from the 3-D/2-D data by summing up over the polar and azimuthal angles. It always has the 6 energy channels of nominal mode: array size {6}.

- Dataset title: Electron, omnidirectional distribution (dataset id ESPCT6∗)

Burst mode: There is one full 3-D electron distribution per spin, with 9 polar directions, 16 azimuthal sectors, and 8 energy channels.

The polar directions 0–2 and 6–8 (those closest to the spin axis, Figure 2) really have only 8 azimuthal sectors per spin; the CSA products artificially double this to simplify handling the data as a rectangular array of size {8,16,9}.

- Dataset title: Electron, 3D distribution (E3DD∗)

Electrons Lite: Since May 2004, an additional 3-D electron product is available in nominal mode. It is the same as the burst mode distribution but for energy channels 1 and 3 only. This was made possible by reprogramming the DPU to download these two channels from the BM dataset onboard (but not otherwise downloaded in NM). This was done at the price of losing the sparse ion and electron 3-D distributions.

For CSA, this product is also emulated in burst mode by simply extracting the two channels from the downloaded burst mode distribution. (It is therefore redundant in BM, but this ensures continuity of the product between the two telemetry modes.)

The array size is {2,16,9} for energy, azimuthal direction, polar direction.

- Dataset title: Electron, 3-D distribution (standard) (L3DD∗)

Nominal mode: Counts are summed over the whole spin, so angular information is limited to 9 polar directions; thus this is often called 2-D data, as reflected in the CSA product name. There are also only 6 energy channels, the top two corresponding to the upper 4 in burst mode. The array size is {6,9}.

- Dataset title: Electron distribution (spin-averaged detector) (E2DD6∗)

Electron Background: one-hour measurements of the steady electron background flux/rates, provided the variations within that interval are consistent with pure Poisson statistical noise. This is described in detail in Section 11 of RAP-CR.

Table 2: A summary table of characteristics for different datasets
showing the number of **E**nergies, **P**olar directions, **A**zimuthal sectors

Species	Dataset title	Dataset name	Data Format					
			NM			BM		
			#E	#P	#A	#E	#P	#A
Electrons	Electron, omni-directional distribution	ESPCT6	6	1	1	6	1	1
	Electron, 3-D distribution (standard)[*]	L3DD	2	9	16	2	9	16
	Electron, 3-D distribution (best)	E3DD	–	–	–	8	9	16
	Electron distribution (spin-averaged detector)	E2DD6 *(for experts)*	6	9	1	–	–	–
	Electron background (spin-averaged detector)	IES_BG *(for experts)*	6	9	1	6	9	1
	Electron 3-D distribution (sparse)[**]	EPADEXm *(for experts)*	2	9[§]	16	2	9	16
Ions	Ion, omnidirectional distribution	HSPCT, ISPCT_He, ISPCT_CNO	8	1	1	8	1	1
	Ion, 3-D distribution (standard)	I3DM_H, I3DM_He, I3DM_CNO	8	12	16	8	12	16
	Proton 3-D distribution (sparse)[***]	IPADEX *(for experts)*	2	12[§]	16	2	12[§]	16
	Ion, 3-D distribution (expanded)[‡]	I3D_H, I3D_He, I3D_CNO *(for experts)*	8	12	16	8	12	16
Atoms	ENA, omnidirectional, SC4, 2001–2002 only	HSPCT_ENA, ISPCT_He_ENA, ISPCT_CNO_ENA	8	1	1	8	1	1
	ENA, 3-D distribution, SC4, 2001–2002 only	I3DM_H_ENA, I3DM_He_ENA, I3DM_CNO_ENA	8	12	16	8	12	16

[*] The product is available since May 2004.

[**] The product ceases after May 2004.

[***] After May 2004 this product is available only in burst mode.

[§] Only 3 directions contain actual data, the others are padded out with fill values. See Figure 9 for a demonstration.

[‡] Expanded 3-D distributions are split into partial distributions according to different accumulation intervals.

Note: the accumulation time for all electron products (except background which is 1 hour) is one spin every spin; the same is true for the omni-directional ions and the sparse 3-D distribution. However, the standard and expanded 3-D ion distributions are accumulated as follows:

SC	BM	NM
2	1 out of 8 spins	1 out of 32 spins
1,3,4	8 out of 8 spins	24 or 40 spins

i.e., in NM, SC1,3,4 the data are accumulated asynchronously over 24 or 40 spins (alternating between records), as shown in Figure 7.

This background is normally from intergalactic cosmic rays, but can also at times be from long-term solar events.

- Electron background, (spin-averaged detector) (`IES_BG*`)

Sparse 3-D: This product exists only until May 2004 (the CSA data files are empty after this), when it was replaced by Electrons Lite (see above). It was originally provided onboard to compensate for the missing 3-D data in NM, and contains fluxes from 3 polar directions for 16 azimuthal sectors, but only for two energy channels. One direction is perpendicular to the magnetic field in that sector, the 2nd is 90° to the first, the 3rd is either parallel or anti-parallel to the spin axis. The other 6 directions are given as fill values. An example of the angle-angle plot created with this product can be seen in Figure 9.

The definitions of the two energy channels have changed several times over the first years of operation; hence 3 separate products must be given, distinguished by an appended m=1, 2, 3:

m	From	To	E1, keV	E2, keV
1	—	May 2001	30- 130	130-406
2	May 2001	July 2002	50- 127	127-406
3	July 2002	April 2004	32- 68	68-127

The above dates are approximate, and vary slightly for each spacecraft. The data files are empty for the times for which they do not apply. No energy corrections are applied for this product.

Strictly speaking this product exists only in NM; in BM it is emulated from BM and it there contains all 9 polar directions. The array size in both modes is {2,16,9}.

- Dataset title: Electron 3-D distribution (sparse) (`EPADEX`m`*`)

5.1.2 Ions

The ion distribution products delivered directly by IIMS can be summarized as follows.
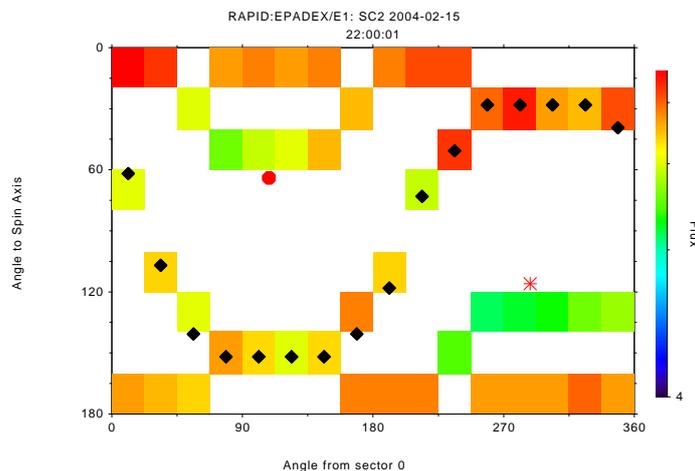
Figure 9: An example of the sparse 3-D electron distribution in s/c coordinates. Black diamonds indicate 90° to the magnetic field, and the red dot and red star mark the calculated direction magnetic field vector (taken from FGM). Therefore, the data obtained in the direction perpendicular to the magnetic field are seen along the black diamonds, the data in second direction, perpendicular to the first, are seen around the red dot and star and eventually the data accumulated in the parallel or anti-parallel to the spin axis direction are seen in the polar sectors 0 (0–20°) and 8 (160–180°).

Omnidirectional: There is an omnidirectional base product for H, with 8 energy channels, which is essentially the sum of all the counts from the all the 3-D directions over one spin. Array size is {8}, the frequency is once per spin.

There are also omnidirectional He and CNO spectra at a rate of one every 4 spins: their array sizes are also {8}.

- These omnidirectional products of course include counts only from those detectors that are functioning, so there will be no contributions from the central head. Similarly, if one of the remaining heads has better efficiency than the other one, it will be weighted correspondingly. Hence the term "omnidirectional" for ions should really be taken to mean "without directional information".

- Dataset titles: Proton (Helium, CNO), omnidirectional distribution (`HSPCT*`, `ISPCT_He*`, `ISPCT_CNO*`)

3-D Data: *The merged full distributions of ion fluxes* for 3 species (H, He, CNO) in 12 polar and 16 azimuthal directions over 8 energy channels. Array size is {8,16,12}.

Each distribution is accumulated over 8 spins, except on spacecraft 2 where they are accumulated over 1 spin out of 8. Because of the limited telemetry rate for RAPID, the transmission to ground takes a much longer than the accumulation time. In burst mode, one can indeed transmit one full distribution over 8 spins, wheareas in nominal mode, it requires 32 spins. There are thus data gaps between the delivered accumulations.

Note that the proper distributions are the partial ones described next. The merged ones are reconstructed from them for the convenience of the users, but may exhibit time-aliasing problems, as shown in Figure 7. The merged distributions are only provided as fluxes, not as count rates.

- Dataset titles: Proton (Helium, CNO), 3-D distribution (standard) (`I3DM_H`, `I3DM_He`, `I3DM_CNO`)

The partial distributions of ion fluxes for 3 species (H, He, CNO) in 12 polar and 16 azimuthal directions over 8 energy channels. Array size is {8,16,12}.

As mentioned in Section 4.2 there is a major bug in the DPU such that for the I3D distributions for SC1, 3, 4 in NM the 3-D distribution is spread over several records. In order to indicate how the partial distributions are to be merged to regenerate the full distribution, a *record key* variable named `Rec_Key` is provided for each record. This is an integer with the following values:

Value	Meaning	Sectors included
11	Rec 1 of 1	0–15 (all)
21	Rec 1 of 2	2–7
22	Rec 2 of 2	0, 1, 8–15
31	Rec 1 of 3	2, 3
32	Rec 2 of 3	0, 1, 4–11
33	Rec 3 of 3	12–15

Note that the value 11 is provided for burst mode and SC2 for which no splitting is done: each record is a complete simultaneous distribution.

For more details, see Appendix A in RAP-ICD.

- Dataset title: Proton (Helium, CNO), 3-D distribution (expanded) (`I3D_H*`, `I3D_He*`, `I3D_CNO*`)

Sparse 3-D: As for the electrons, there is a sparse 3-D hydrogen distribution available every spin, with 3 polar directions per sectors, which vary with the magnetic field. It too is expanded to fill the complete 3-D array

with fill values for those directions not measured. The array size is {2,16,12}.

As of May 2004, this product exists only in burst mode.

- Dataset title: Proton 3-D distribution (sparse) (`IPADEX*`)

5.1.3   Energetic Neutral Atoms

For the energetic neutral atoms (ENA) mode on IIMS, a 10 kV voltage is applied across the entry aperature, sweeping out ions (up to ~150 keV), allowing only energetic atoms to enter and to be processed.

The ENA mode was only ever applied to SC4 at certain times in the solar wind, and then only before May 2002. (See table in Appendix D of RAP-CR.) It never appeared that any useful data were obtained, especially with the problems of the IIMS loss of the central head. However, these datasets are provided for completeness, and so that future uses can decide for themselves. No count rate products are provided since they are included in the unprocessed ion products.

Omnidirectional: Analogous to the ion omnidirectional data, 8 energy channels summed over all directions in one spin. Array size {8}, frequency once per spin.

- Dataset titles: Hydrogen (Helium, CNO) atoms, omni-directional distribution (`HSPCT_ENA`, `ISPCT_He_ENA`, `ISPCT_CNO_ENA`)

3-D Data: Analogous to the merged ion 3-D distributions, in 12 polar, 16 azimuthal directions and 8 energy channels. Array size {8,16,12}. Accumulation times the same as for the ions.

- Dataset titles: Hydrogen (Helium, CNO) atoms, 3-D distribution (`I3DM_H_ENA`, `I3DM_He_ENA`, `I3DM_CNO_ENA`)

5.1.4   Pitch Angle Distributions

The pitch angles for electrons and ions are delivered based on the 5-vectors-per-second (5VPS) FGM data. Each distribution is accompanied by the GSE components of the magnetic field averaged over the data interval plus a quality flag. This flag is derived from the normalized variance of the field such that it is 1 for steady (constant) field and 0 for extremely variable.

Electrons: Differential fluxes in 9 pitch angle bins (0–180°) are available in burst mode, 8 energy channels and after May 2004 in nominal mode, 2 non-contiguous energy channels. The distribution is provided once per spin.

- Dataset title: Electron Pitch Angle distribution (standard, best) (`PAD_L3DD`, `PAD_E3DD`)

Ions: Differential fluxes in 9 pitch angle bins (0-180°) and 8 energy channels.

Ion pitch angle distributions are provided for
SC2: over 1 spin every 32/8 spins (NM/BM)
SC1, SC3, SC4, BM: over 8 spins once every 8 spins
SC1, SC3, SC4, NM: 8 spins with asynchronous sectors over 24 or 40 spins (a result of the bug illustrated in Figure 7)

- Dataset title: Proton (Helium, CNO) Pitch Angle distribution (standard) (`PAD_H`, `PAD_He`, `PAD_CNO`)

5.1.5   Direct Events

A limited number of unprocessed ion events are output for each spin, allowing exact identification of particles with energy and time-of-flight resolution of 256 bins each, 16 azimuthal sectors and 16 polar directions. The 256 bins for energy cover the range from 0 to 1500 keV and for TOF from 0 to 80 ns. Both scales are linear. The events can be classified by species and energy channel according to their location in the E–TOF space of Figure 4. There are up to 20 (NM) or 106 (BM) events for each spin.

For more details, especially about the prioritization scheme for the outputted species, see RAP-ICD, Section 5.2.7 and Appendix B.

- Dataset title: Direct Events (DE)

5.1.6 Ion Matrix

Ions count rates for various masses and energies at low time resolution (64 spins) are provided with the MTRX data product, described in Section 13.2 of RAP-CR. This is an array of 32 masses and 64 energies-per-mass, converted from the E–TOF space of the direct events by means of preprogrammed curves for different ions. However, since these curves for the higher masses are not correct at lower energies, it is by no means trivial to determine what the true mass and energy are for each array element.

- Dataset title: Full ion mass-energy matrix, count rates (MTRX_R)

To get around this problem and to provide the general user with a useful product, we produce a *reduced matrix* RMTRX that contains 8 energy channels for 5 ion species: H, He, CNO, Si, Fe, taken as sums over selected areas in the MTRX array. The specialist information is therefore already built into this product. It too, along with a table of the energy channel values, are given in Section 13.2 of RAP-CR.

- Dataset title: Simplified ion mass-energy matrix, count rates (RMTRX_R)

5.2 Auxiliary Data

Some additional datasets are provided to assist users with the interpretations; their derivation requires detailed knowledge of the RAPID location on the spacecraft, the spin axis, and sun sensor. Thus all this is worked out for the user, as separate products.

Flow directions: For each of RAPID's 9×16 (electrons) and 12×16 (ions) polar-azimuth directions, the GSE coordinates of the *flow* vector at their centers are provided. Since these values change very slowly, they are only given once per hour. (Note: *flow* direction is the opposite of the instrument *look* direction.)

- Dataset title: Electron (Ion) Flow direction matrix, RAPID to GSE rotation (EFLOW_GSE, IFLOW_GSE)

SC-GSE rotation matrix: Provided in the same files as the flow directions is the actual 3×3 rotation matrix to do a general transformation to GSE from the RAPID spacecraft frame (θ = angle to spin axis, ϕ = sector $\times 22.5°$). See Appendix E for usage.

- Dataset title: Electron (Ion) Flow direction matrix, RAPID to GSE rotation (EFLOW_GSE, IFLOW_GSE)

Pitch Angles: For each of the electron and ion polar-azimuth flow directions, the angle to the magnetic field (pitch angle) plus a magnetic azimuth is provided; this is done for each spin. These are produced using the FGM_5VPS (5 vectors per second) data.

- Dataset title: Electron (Ion) pitch angle assignment matrix (EPITCH, IPITCH)

What is necessary in order to plot 3-D angle-angle plot

- One can create angle-angle plots from 3-D distributions (in any units): E3DD, L3DD, I3DM_H, I3DM_He, I3DM_CNO, I3D_H, I3D_He, I3D_CNO, EPADEXm, IPADEXm
- EFLOW_GSE or IFLOW_GSE: the rotation matrix for rotation from SC to GSE coordinates
- Spin resolution or 5VPS FGM magnetic field vector: in the case the magnetic field direction will be plotted (see white and red dots in Figure 10).

5.3 Status Flags

The key two datasets for knowing the instrument status are CAVEATS and DSETTINGS.
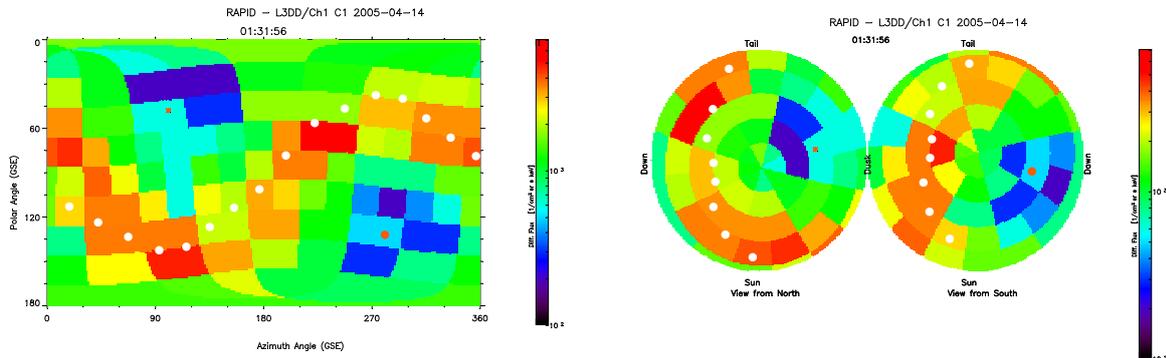
Figure 10: Left: 3-D electron distribution from L3DD data in GSE showing 9 polar directions and 16 azimuthal sectors. Right: The same data but in a bispherical view, whereas the left spheres on both plots show northward flow and the right southward. White dots indicate 90° to the magnetic field, and the red dot and red star mark the calculated direction magnetic field vector.

The CAVEATS dataset text contains warnings or information on data gaps. Some of these are generated automatically by the processing software, while others are copied from a master list maintained by the RAPID Team. The daily caveat files contain only those caveats that are relevant to that one day.

Each caveat text has an associated *time range* which is always truncated to fit within the time limits of the given file. This means it does not represent the true overall time limitation of the text. In such cases, the text itself specifies when the warning starts and stops.

The DSETTINGS dataset contains a subset of the housekeeping data, 11 variables in all, for the most important aspects of the instrument status including telemetry mode, multichannel plate voltages, electron integration time, ion accumulation mode. These variables are described in Section 5.2.2 of RAP-ICD, as well as in the dataset metadata.

For DSETTINGS, there is one record every time at least one of the 11 variables changes value, together with a *time range*. There is also an obsolete SETTINGS dataset which contains all 11 values plus time stamp, for *every single spin*, making it unnecessarily very large. It is recommended to use the newer DSETTINGS dataset.

5.4 Dataset Version

The calibration version can be found in the data files. There is a metadata parameter called DATASET_VERSION, which for RAPID is a 4-digit code, which is slightly different for electrons and ions.

Calibration version
Pedestal determination (e), Cal subset (ions)
Spectrum correction
Background subtraction
X X X X
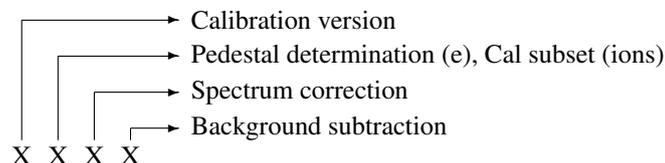
Calibration version is currently 4 (4th release, Section 5.3 of RAP-CR) for both IES and IIMS, for all deliveries after June 2018; older datasets of version 3 at CSA will eventually be replaced by reprocessing and redelivery. Versions 1 and 2 have long been replaced at CSA and any existing downloaded datasets with these numbers should be deleted and downloaded once more.

Pedestal determination for electrons; how the pedestal (Figure 3) is determined: 0 for no correction, 1 for the "stepping" method, the only method used at the moment, but other methods may be added in the future.

Cal subset for ions; for internal RAPID usage: the data at CSA always have the value 2.

Spectrum correction how the varying energy thresholds between detectors, spacecraft, and (for electrons) integration times are corrected to a uniform set of values. The pedestal shift for electrons is also corrected with spectral shifting. Possible values are: 0 for no correction, 2 and 3 for power law fitting between two adjacent channels. With 2, the pedestal shift is the spin average, while for 3, it is done for each sector. So far only 2 is used.

Background subtraction 0 for no subtraction; 3 for removal of solar noise on SC3 (Section 4.1).

5.5 Quality Flag

Every CSA RAPID data product contains the quality flag. In fact, this is the calibration version for a given calibration set (constant number). The user should see the caveat files for detailed issues.

5.6 Graphical Products

RAPID summary plots are available for differential fluxes. In Figure 11 we present an example plot of Cluster 1 from January 25, 2005, from 12:00 to 18:00 UT, at 1-min time resolution. The top four panels show omnidirectional differential energy flux spectra of electrons, hydrogen, helium, and CNO. On the right hand side of each plot panel a colour bar defines the colour code for the spectra. This range is autoscaled, which has to be considered when comparing different plots.

The second part of the plot (panels 5-7) reflects the IES and IIMS instrument settings. For more information about instrument settings and their meaning see the description in Section 3 and RAP-ICD.

At the bottom of the summary plot orbit information in GSE coordinates is given.

The Summary Plots can be downloaded from CSA as part of the RAPID *ancillary* data or viewed under the CSA Quicklook plots. They may also be obtained from the MPS web site at `http://www2.mps.mpg.de/cgi/rapid/sumplot.cgi`.

6 Recommendations

Most straightforward to use are the omnidirectional particle fluxes for ions and electrons.

A summary of the RAPID Datasets at the CSA is listed in Appendix A.

A guide on calculations of the RAPID partial moments can be found in Appendix B.

Conversion factors between differential flux and phase space density are listed in Appendix C.

6.1 Usability issues

Important events in the RAPID history: a list of such events is given in Appendix G; it includes when voltage levels were changed, when electron channel definitions changed, and when special operations (NM3, tilt campaign) took place, and when parts of the instruments ceased to function.

Regions where the instrument operates well: These are the plasma sheet, magnetosheath, magnetopause, cusp, bow shock, upstream region, in cases where for ions the main plasma flow direction does not coincide with the look direction of the dead sensor.

Regions where there are issues: The radiation belts is a region where a user must be careful with the data analysis. In this region the pileup problems can lead to a flat spectrum, see Section 3.2 and Figure 6. Here too there can be problems with the auto-switching of the integration time and thus erroneous jumps in the fluxes, see the same section and Figure 5.
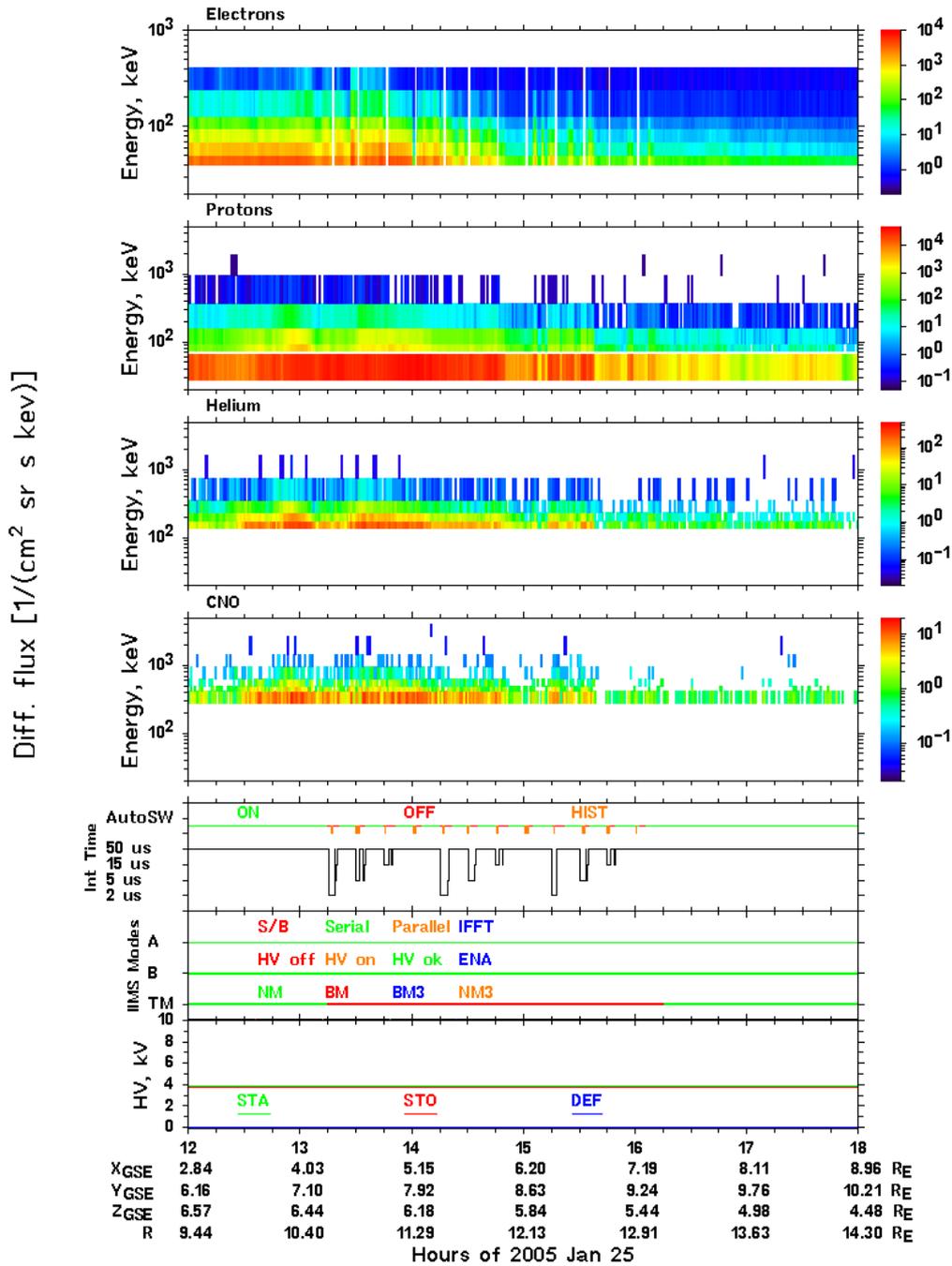
Figure 11: Example of a CSA RAPID summary plot. Panels 1–4 show from top to bottom differential fluxes of ESPCT, HSPCT, ISPCT_He, and ISPCT_CNO. Panels 5–7 display several instrument settings.

Additionally at ∼3-5 L-shells more energetic ions and electrons can penetrate the IES instrument, see Figure 12.

The IIMS instrument is not so sensitive to the penetrating particles because of time-of-flight filtering. The pileup effects, from both penetrating particles and high count rates can be detected and will be flagged in future.

Solar Proton Events: can also produce penetrating radiation that distorts the instrument's behavior, see an example in Figure 13.
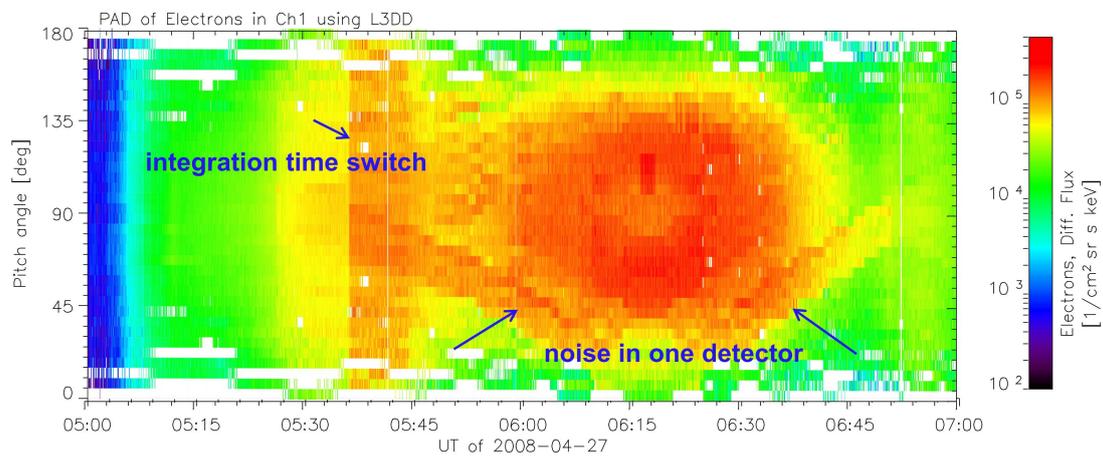
Figure 12: An example of the electron data contamination in the radiation belts. In the pitch-angle distribution of the electrons one could see stripes denoted as the noise in one detector. The fact that this noise appears only in the radiation belts implies that the contamination is from penetrating particles. The sharp enhancement of the electron flux at the integration time switch is not related to the contamination problem.
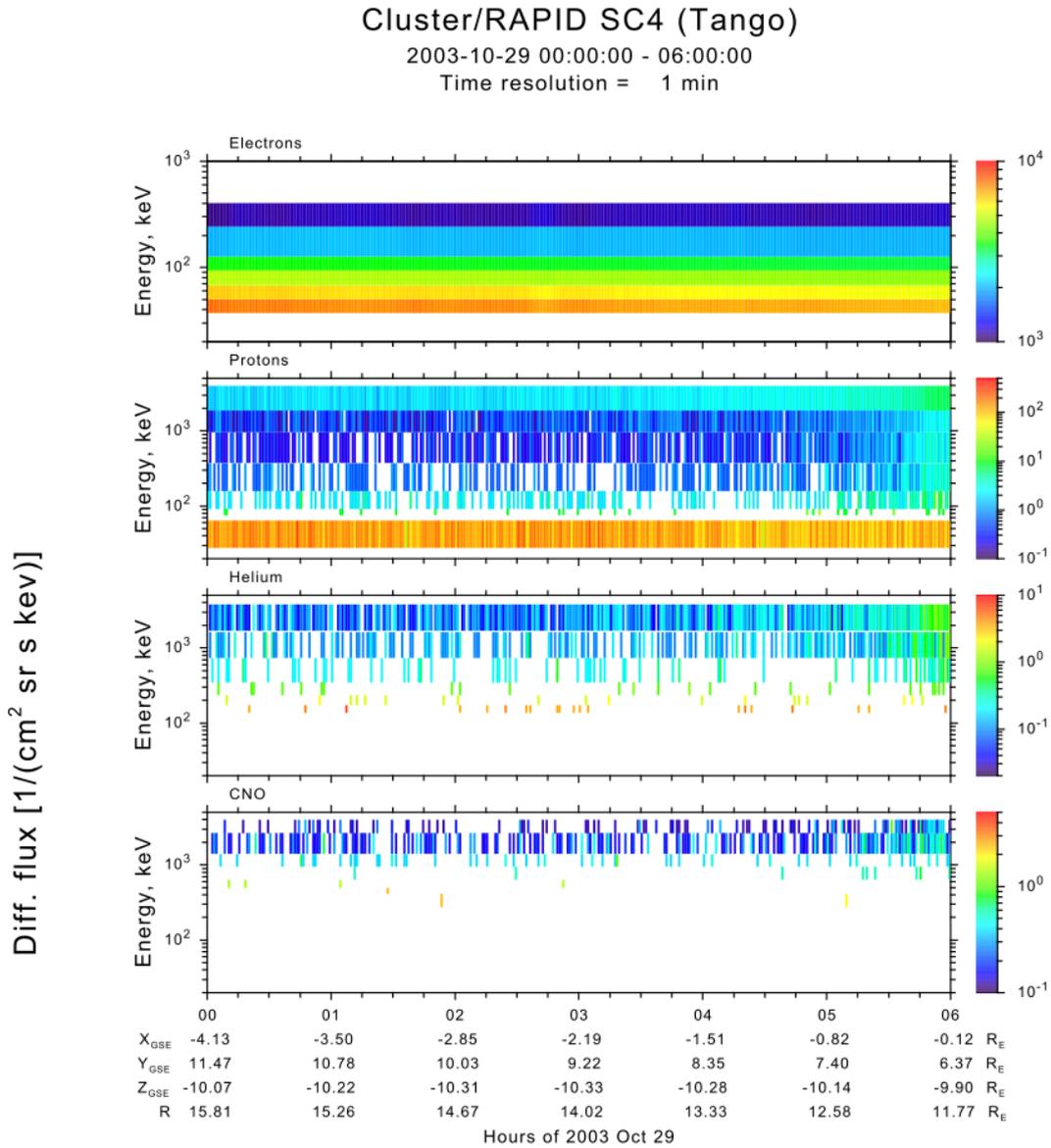
Figure 13: An example of the effects which produce penetrating particles during the Halloween solar proton event. Electrons do not show sensible measurements. Ion intensities increase with the energy, when they expected to decrease towards the higher energy channels.

Appendices

A   Summary of RAPID Datasets at CSA

Table 3: A summary table of RAPID datasets (Dataset ids with $*$ also have a version with _R for raw count rates, those with $\dagger$ are available only as _R).

Dataset title	Dataset ID
Science	
Particle Distribution	
Electron, omnidirectional distribution	ESPCT6$*$
Electron, 3-D distribution (standard)	L3DD$*$
Electron, 3-D distribution (best)	E3DD$*$
Proton, omnidirectional distribution	HSPCT$*$
Proton, 3-D distribution (standard)	I3DM_H
Helium, omnidirectional distribution	ISPCT_He$*$
Helium, 3-D distribution (standard)	I3DM_He
CNO, omnidirectional distribution	ISPCT_CNO$*$
CNO, 3-D distribution (standard)	I3DM_CNO
Array of count rates over 32 masses $\times$ 64 energy-per-mass elements, over 64 spins	MTRX_R†
Reduced version of above, (see Section 5.1.6), array of 5 masses $\times$ 8 energies	RMTRX_R†
Pitch Angle	
Electron Pitch Angle distribution (standard)	PAD_L3DD
Electron Pitch Angle distribution (best)	PAD_E3DD
Proton Pitch Angle distribution (standard)	PAD_H
Helium Pitch Angle distribution (standard)	PAD_He
CNO Pitch Angle distribution (standard)	PAD_CNO
Ancillary	
Caveats	CAVEATS
Instrument settings	DSETTINGS
Summary Plot	SUMPLOT_D
Electron Flow direction matrix, RAPID to GSE rotation	EFLOW_GSE
Ion Flow direction matrix, RAPID to GSE rotation	IFLOW_GSE
Electron pitch angle assignment matrix	EPITCH
Ion pitch angle assignment matrix	IPITCH
Particle Distribution	
Electron distribution (spin-averaged detector)	E2DD6$*$
Electron background (spin-averaged detector)	IES_BG$*$
Electron 3-D distribution (sparse): 2001/Feb – 2001/May	EPADEX1$*$
Electron 3-D distribution (sparse): 2001/May - 2002/Jul	EPADEX2$*$
Electron 3-D distribution (sparse): 2002/Jul - 2004/Apr	EPADEX3$*$
Proton 3-D distribution (sparse)	IPADEX$*$

continued …

Table 3: RAPID datasets, *continued*

Dataset title	Dataset ID
Proton, 3-D distribution (expanded)	I3D_H*
Helium, 3-D distribution (expanded)	I3D_He*
CNO, 3-D distribution (expanded)	I3D_CNO*
Hydrogen atoms, omnidirectional distribution	HSPCT_ENA
Helium atoms, omnidirectional distribution	ISPCT_He_ENA
CNO atoms, omnidirectional distribution	ISPCT_CNO_ENA
Hydrogen atoms, 3-D distribution (standard)	I3DM_H_ENA
Helium atoms, 3-D distribution (standard)	I3DM_He_ENA
CNO atoms, 3-D distribution (standard)	I3DM_CNO_ENA
Diagnostics	
Direct Events	DE
Ion diagnostics, SGL1, count rates, nominal mode	SGL1
Ion diagnostics, SGL1, count rates, burst mode	SGL1_BM
Ion diagnostics, SGL2, count rates	SGL2
Ion diagnostics, SGL3, count rates	SGL3
IES pedestal counts in nominal mode	PED_NM
IES pedestal counts in burst mode	PED_BM
IES pedestal positions in nominal mode	PEDPOS_NM
IES pedestal positions in burst mode	PEDPOS_BM
IES Histogram data	HIST
Miscellaneous	
Housekeeping data	HK
Preliminary Energetic Electron, Proton, and Ion Flux, spin resolution	C(n)_PP_RAP
Preliminary Energetic Electron, Proton, and Ion Flux, 1 minute resolution	C(n)_SP_RAP

B   Partial moments

The moments of the velocity distribution function, $f(\mathbf{v})$, of a given particle species are calculated as

$$M_n = \int f(\mathbf{v})\mathbf{v}^n d^3 v \tag{1}$$

where $\mathbf{v}^n$ denotes the n-fold dyadic product, a tensor of rank n, and $d^3 v$ is the volume element in velocity space.

Therefore the zero-, first-, and second-order moments will be correspondingly the number density, n, the bulk flow velocity $\mathbf{V}$, and the pressure tensor P.

It is common to use as the measurable quantity for particle counters the differential flux $j(E, \Omega)$ for particles of energy E, within a solid angle $d\Omega$. The relation between the distribution function and the differential flux is:

$$j(E, \Omega) = \frac{v^2}{m} f(\mathbf{v}) = \frac{2E}{m^2} f(\mathbf{v}) \tag{2}$$

Since $d^3 v = \int d\phi \int d\theta \sin\theta \int dv v^2$ and $v = \sqrt{2E/m}$ then $d^3 v = \int d\phi \int d\theta \sin\theta \int dE \sqrt{2E}/m^{3/2}$, where $d\Omega = d\phi \int d\theta \sin\theta$. Here E is the effective energy or in practice the geometric mean of a given energy channel, (for more details see chapter about phase space density), and dE is the energy width of an energy channel. Using these relations we can derive the moments as functions of measurable quantities.

B.1   Density

For the density (the zero-order moment) calculated from the 3-D data the following formula can be used:

$$n[\mathrm{cm}^{-3}] = 0.2284 \cdot 10^{-7} \sqrt{m[\mathrm{amu}]} \sum_\phi \Delta\phi \sum_\theta \Delta\theta \sin\theta \sum_E \frac{\Delta E[\mathrm{keV}]}{\sqrt{E[\mathrm{keV}]}} j[\mathrm{cm}^{-2}\mathrm{sr}^{-1}\mathrm{s}^{-1}\mathrm{keV}^{-1}] \tag{3}$$

In case of using omnidirectional flux:

$$\sum_\phi \Delta\phi \sum_\theta \Delta\theta \sin\theta = 4\pi \tag{4}$$

Note: The central head on the ion detector is damaged therefore one can not use 3-D data for calculation of the ion number density.

B.2   Velocity

The components of the bulk flow velocity (the first-order moment) are expressed as

$$V_x[\mathrm{km\ s}^{-1}] = 10^{-5} \frac{1}{n[\mathrm{cm}^{-3}]} \sum_\phi \Delta\phi \cos\phi \sum_\theta \Delta\theta \sin^2\theta \sum_E \Delta E[\mathrm{keV}] j[\mathrm{cm}^{-2}\mathrm{sr}^{-1}\mathrm{s}^{-1}\mathrm{keV}^{-1}]$$

$$V_y[\mathrm{km\ s}^{-1}] = 10^{-5} \frac{1}{n[\mathrm{cm}^{-3}]} \sum_\phi \Delta\phi \sin\phi \sum_\theta \Delta\theta \sin^2\theta \sum_E \Delta E[\mathrm{keV}] j[\mathrm{cm}^{-2}\mathrm{sr}^{-1}\mathrm{s}^{-1}\mathrm{keV}^{-1}] \tag{5}$$

$$V_z[\mathrm{km\ s}^{-1}] = 10^{-5} \frac{1}{n[\mathrm{cm}^{-3}]} \sum_\phi \Delta\phi \sum_\theta \Delta\theta \sin\theta \cos\theta \sum_E \Delta E[\mathrm{keV}] j[\mathrm{cm}^{-2}\mathrm{sr}^{-1}\mathrm{s}^{-1}\mathrm{keV}^{-1}]$$

Note: For calculation of the bulk velocity the only 3-D data can be used as one needs the direction information for this. Therefore the bulk velocity can be calculated only for electrons as ions have lack of measurements in the central head.

B.3   Pressure

The diagonal terms of the kinetic pressure tensor (the second-order moment) are the following

$$P_{xx}[\text{nPa}] = 0.731 \cdot 10^{-8}\sqrt{m[\text{amu}]} \sum_\phi \Delta\phi \cos^2\phi \sum_\theta \Delta\theta \sin^3\theta \sum_E \Delta E[\text{keV}]\sqrt{E[\text{keV}]}\, j[\text{cm}^{-2}\text{sr}^{-1}\text{s}^{-1}\text{keV}^{-1}]$$

$$P_{yy}[\text{nPa}] = 0.731 \cdot 10^{-8}\sqrt{m[\text{amu}]} \sum_\phi \Delta\phi \sin^2\phi \sum_\theta \Delta\theta \sin^3\theta \sum_E \Delta E[\text{keV}]\sqrt{E[\text{keV}]}\, j[\text{cm}^{-2}\text{sr}^{-1}\text{s}^{-1}\text{keV}^{-1}]$$

$$P_{zz}[\text{nPa}] = 0.731 \cdot 10^{-8}\sqrt{m[\text{amu}]} \sum_\phi \Delta\phi \sum_\theta \Delta\theta \sin\theta \cos^2\theta \sum_E \Delta E[\text{keV}]\sqrt{E[\text{keV}]}\, j[\text{cm}^{-2}\text{sr}^{-1}\text{s}^{-1}\text{keV}^{-1}]$$

(6)

For the isotropic pressure

$$P[\text{nPa}] = 4\pi\frac{2}{3}0.51767 \cdot 10^{-8}\sqrt{m[\text{amu}]} \sum_E \Delta E[\text{keV}]\sqrt{E[\text{keV}]}\, j[\text{cm}^{-2}\text{sr}^{-1}\text{s}^{-1}\text{keV}^{-1}] \qquad (7)$$

Note: For calculation of the pressure tensor only 3-D electron data could be used. An isotropic pressure can be derived from both electron and ion omnidirectional fluxes.

C   Phase Space Density Conversion Factors

A set of fixed conversion factors between differential flux j and phase space density f based on the mean energies E_g of each channel, is listed in Table 4. More details on its calculation can be found in RAP-CR.

Chan	E_g	f/j	E_g	f/j
		Protons		Helium
1	42.23	1.271×10^{-2}	64.18	1.338×10^{-1}
2	83.32	6.445×10^{-3}	154.0	5.576×10^{-2}
3	121.3	4.426×10^{-3}	201.2	4.269×10^{-2}
4	244.3	2.197×10^{-3}	287.2	2.991×10^{-2}
5	599.8	8.953×10^{-4}	508.6	1.689×10^{-2}
6	1340.	4.005×10^{-4}	1100.	7.806×10^{-3}
7	2748.	1.954×10^{-4}	2533.	3.392×10^{-3}
8	4007.	1.340×10^{-4}	3799.	2.261×10^{-3}
		Oxygen		Electrons
1	151.6	9.066×10^{-1}	44.49	5.284×10^{-9}
2	337.0	4.079×10^{-1}	58.64	4.487×10^{-9}
3	454.0	3.028×10^{-1}	80.22	3.872×10^{-9}
4	563.6	2.439×10^{-1}	109.7	3.517×10^{-9}
5	777.7	1.767×10^{-1}	149.7	3.402×10^{-9}
6	1157.	1.187×10^{-1}	207.2	3.556×10^{-9}
7	1931.	7.117×10^{-2}	286.6	4.080×10^{-9}
8	3267.	4.207×10^{-2}	369.8	4.883×10^{-9}

Table 4: Conversion factors from differential flux j ($cm^{-2}s^{-1}sr^{-1}keV^{-1}$) to phase space density f ($km^{-6}s^3$). The ratio f/j is listed; to obtain f, multiple the j value by this ratio.

D   Calculations of Adiabatic Invariants

This Section is based on work by Artem Smirnov [Smirnov et al., 2020].

Conversion of the measured electron differential flux $j(E, \alpha, \mathbf{r}, t)$ as a function of energy, pitch angle, spacecraft position, and time to phase space density (PSD) $f(\mu, K, L^*, t)$ as a function of three adiabatic invariants and time is done in the following steps.

Step 1. The second adiabatic invariant. The RAPID/IES instrument allows the calculation of pitch angles for energy channels 1 and 3 starting from 2004 (PAD_L3DD product). Pitch angle distributions in radiation belts are mostly having the so-called "pancake" shape, with most particles concentrated around the perpendicular pitch-angles. At these pitch-angles, $\alpha = 90°$, we obtain the best coverage for the phase space density. We refer to the corresponding differential fluxes as $j_{ch.1,90°}$ and $j_{ch.3,90°}$. In this case the value of the second invariant K is assumed to be zero.

Step 2. Calculate the first adiabatic invariant μ and PSD values for $j_{ch.1,90°}$ and $j_{ch.3,90°}$ using the following formulas:

$$\mu_i = \frac{E_i(E_i + 2m_0c^2)}{2m_0c^2 B} \cdot 10^5 \left[\frac{\text{MeV}}{G} \right] \tag{8}$$

where E_i is energy in MeV for channel $i = 1, 3$, m_0c^2 is the rest energy of the particle (for electrons equal to 0.511 MeV) and B is the magnetic field magnitude measured by the satellite in nT;

$$f_i = \frac{j_{ch.i,90°}}{E(E + 2m_0c^2)} \cdot \left[1.66 \times 10^{-10} \right] \times 200.3 \tag{9}$$

where f_i is the phase space density in GEM (Geospace Environment Modeling) units $(\text{c/MeV/cm})^3$ for channel $i = 1, 3$, $j_{ch.i,90°}$ is electron differential flux in units $\text{cm}^{-2}\text{sr}^{-1}\text{s}^{-1}\text{keV}^{-1}$.

Step 3. Calculations of L* parameter. The L* coordinate is equivalent to the third adiabatic invariant. The values of L* with 1 minute resolution can be obtained through the Cluster Science Archive (LSTAR product).

For calculations of L* it is necessary to specify the satellite position, magnetic field model (since the fluxgate magnetometer onboard gives the magnetic field value at only one point) and geomagnetic/magnetospheric conditions. For the Lstar product, calculations were performed using the IRBEM library (make_lstar function). Tsyganenko-89 magnetic field model with Kp-index as an input was employed.

Thus, one gets the value of PSD as a function of adiabatic invariants $f(\mu, K, L^*, t)$.

E   RAPID to GSE Rotation Matrix

In Section 5.2, the products `EFLOW_GSE` and `IFLOW_GSE` are described, which give the GSE coordinates for each of the 9×16 (electrons) or 12×16 (ions) detector-sector combinations in the 3-D datasets, shown in Figure 2. These detectors and sectors are fixed in the spacecraft coordinate system, and must be transformed to GSE by means of the rotation matrix included in the two datasets.

Note that:

- The GSE coordinates given are the *polar* angle from the Z-axis ($0 \rightarrow 180°$) and the *azimuthal* angle from the X-axis ($-180 \rightarrow +180°$).

- The direction refers to the *flow* directions of particles detected, i.e., it is opposite to the direction in which the detector is pointing!

- The direction corresponds to the middle of each sector/detector range.

The rotation matrix alone would be sufficient to generate all the flow directions; however the results are given as a convenience to the user, and to eliminate many of the intrinsic ambiguities. A description of how to apply the rotation matrix properly is found in RAP-GSE, and a summary is given here.

E.1   The RAPID Spacecraft Frame

Let us define the RAPID coordinate system to be relative to unit vectors $\hat{u}$ along sector 0.0, $\hat{v}$ along sector 4.0, and $\hat{w}$ along the spin axis (Figure 14). The look direction for the middle of detector d in sector s has the angular coordinates

$$\theta = \pi \frac{d + 0.5}{D} \qquad \phi = 2\pi \frac{s + 0.5}{16} \tag{10}$$

where D is 12 for ions and 9 for electrons. The vector $\mathbf{L}$ for the look direction is

$$\mathbf{L} = a\hat{u} + b\hat{v} + c\hat{w} \tag{11}$$

where the cartesian coordinates are

$$\begin{aligned}
a &= \sin\theta \cos\phi \\
b &= \sin\theta \sin\phi \\
c &= \cos\theta
\end{aligned} \tag{12}$$

E.2   The Rotation Matrix

The 3×3 matrix for rotating from the RAPID system to GSE is given in each record of the `EFLOW_GSE` and `IFLOW_GSE` products. This matrix is determined using the following factors:

- The location of RAPID on the spacecraft (fixed!)

- The position of sector 0.0 relative to the sun pulse (has an ideal value but can vary); given in the RAPID housekeeping data.

- The GEI location of the spin axis, as given in the attitude files (varies very slowly, is updated every few days).

- The spin phase corresponding to the occurrence of the sun pulse, also in the attitude files (can vary slightly).

The GEI coordinates for the spin axis are converted to GSE using standard algorithms [e.g. *Hapgood*, 1992, and references therein]. We can then determine the GSE coordinates of both the spin axis and the RAPID sector 0.0, which is sufficient to generate the rotation matrix M: its columns are simply the three vectors $\hat{u}$, $\hat{v}$, $\hat{w}$, expressed as GSE cartesian coordinates.
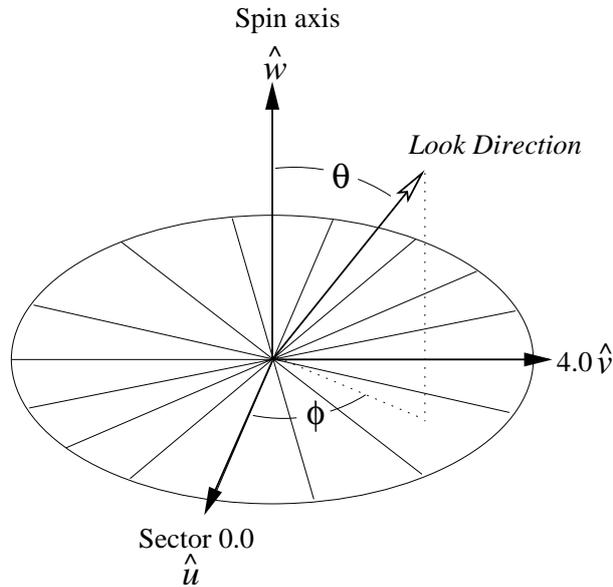
Figure 14: The RAPID spacecraft coordinate system, fixed to the spin axis ($\hat{w}$) and the start of the 16 spin sectors ($\hat{u}$). An arbitrary look direction has angular coordinates θ and ϕ.

The flow vector $\mathbf{F}_{gse}$ is then

$$\mathbf{F}_{gse} = - \begin{pmatrix} M_{11} & M_{12} & M_{13} \\ M_{21} & M_{22} & M_{23} \\ M_{31} & M_{32} & M_{33} \end{pmatrix} \begin{pmatrix} a \\ b \\ c \end{pmatrix} \tag{13}$$

or generally,

$$\mathbf{F}_{gse} = -\mathsf{M} \cdot \mathbf{L}_{rap}$$

Note the minus sign to convert from look to flow direction!

The components of M are given in the CEF files by *row*, i.e. as $M_{11}, M_{12}, \ldots, M_{32}, M_{33}$.

E.3 Example

As an example, let us take a record from `EFLOW_GSE` for SC1 on 2001-08-22. It starts with the time stamp and the 9 values of M:

```
2001-08-22T03:30:44.501Z,
  0.49308, -0.86430, -0.09930, -0.86976, -0.49232, -0.03377, -0.01970, 0.10302, -0.99448,
```

Let us calculate the flow direction for detector 2, sector 3 (both counting from 0), which from Eqn. 10 gives us $\theta = 50°$ and $\phi = 78.75°$, and from Eqn. 12

$$a = 0.1494 \quad b = 0.7513 \quad c = 0.6428$$

We now apply Eqn. 13 to get

$$\begin{pmatrix} 0.49308 & -0.86430 & -0.09930 \\ -0.86976 & -0.49232 & -0.03377 \\ -0.01970 & 0.10302 & -0.99448 \end{pmatrix} \begin{pmatrix} -0.1494 \\ -0.7513 \\ -0.6428 \end{pmatrix} = \begin{pmatrix} 0.6395 \\ 0.5216 \\ 0.5648 \end{pmatrix}$$

The flow vector on the right is in GSE coordinates and corresponds to $\theta_{gse} = 55.61°$ and $\phi_{gse} = 39.20°$, the same values that are listed later in this record for this detector/sector combination.

```
    11.69, 30.59, 50.31, 70.16, 90.04, 109.93, 129.78, 149.50, 168.38,
    13.52, 32.77, 52.56, 72.44, 92.34, 112.24, 132.11, 151.85, 170.56,
```

```
14.89, 34.52, 54.41, 74.34, 94.28, 114.23, 134.14, 153.98, 172.91,
15.74, 35.64,  55.61 , 75.59, 95.58, 115.56, 135.54, 155.48, 175.04,
...
77.72, 98.08, 103.33, 106.17, 108.36, 110.55, 113.39, 118.67, 139.22,
61.94, 77.07, 81.48, 83.98, 85.97, 88.02, 90.78, 96.19, 121.48,
47.09, 57.04, 60.17, 62.01, 63.52, 65.10, 67.31, 71.90, 99.59,
32.70, 37.59,  39.20 , 40.17, 40.97, 41.83, 43.05, 45.71, 67.78,
...
```

E.4   Things to Note

The rotation matrices given in the two products are identical, for the same spacecraft and time. It is only the array sizes of the resulting flow matrices that are different for ions and electrons.

We have assumed here that the spin axis is identical with the body reference axis of the spacecraft. Strictly speaking, this is not true, and the attitude files also contain information on this deviation. However, these are very small ($< 0.05°$) and so have been neglected.

As a result of the fact that the spacecraft spin axis is closely aligned to the *negative* GSE Z-axis, the rotation matrix is nearly equal to its transpose, or inverse. This means that if one applies it in the wrong direction, a common and understandable error (e.g. by filling it by columns instead of rows), the result does not appear immediately to be utterly wrong. It is for this reason that we provide the correct results, and also emphasize how the matrix is to be filled and applied.

F List of Times when NM3 Mode was Used

From Planing Periods 166–211, SC2

SC		Day	Time	Planning Period	Duration (hours)
2	ON	2003-07-26	09:50:00	166	
	OFF	2003-07-28	20:05:00	167	58.25
2	ON	2003-08-04	21:50:00	168	
	OFF	2003-08-07	07:15:00	168	57.42
2	ON	2003-08-09	16:00:00	168	
	OFF	2003-08-09	17:30:00	169	1.50
2	ON	2003-08-14	10:30:00	169	
	OFF	2003-08-14	12:05:00	169	1.58
2	ON	2003-08-21	13:35:00	170	
	OFF	2003-08-21	14:37:00	170	1.03
2	ON	2003-08-23	22:35:00	170	
	OFF	2003-08-25	06:37:00	171	32.03
2	ON	2003-08-25	15:46:00	171	
	OFF	2003-08-26	08:55:00	171	17.15
2	ON	2003-08-28	16:40:00	171	
	OFF	2003-08-28	18:15:00	171	1.58
2	ON	2003-09-02	11:05:00	172	
	OFF	2003-09-02	12:40:00	172	1.58
2	ON	2003-09-04	19:55:00	172	
	OFF	2003-09-04	21:45:00	172	1.83
2	ON	2003-09-07	05:30:00	172	
	OFF	2003-09-07	07:05:00	173	1.58
2	ON	2003-09-09	14:10:00	173	
	OFF	2003-09-09	15:08:00	173	0.97
2	ON	2003-09-12	02:50:00	173	
	OFF	2003-09-14	10:15:00	174	55.42
2	ON	2003-09-16	19:05:00	174	
	OFF	2003-09-19	02:55:00	174	55.83
2	ON	2003-09-21	11:40:00	174	
	OFF	2003-09-21	13:15:00	175	1.58
2	ON	2003-09-23	20:50:00	175	
	OFF	2003-09-23	22:40:00	175	1.83
2	ON	2003-09-26	06:10:00	175	
	OFF	2003-09-26	07:45:00	175	1.58
2	ON	2003-09-28	14:50:00	175	
	OFF	2003-09-28	15:48:00	175	0.97
2	ON	2003-10-03	09:15:00	176	
	OFF	2003-10-03	10:45:00	176	1.50
2	ON	2003-10-05	19:55:00	177	
	OFF	2003-10-06	10:05:00	177	14.17

continued…

SC		Day	Time	Planning Period	Duration (hours)
2	ON	2003-10-06	11:35:00	177	
	OFF	2003-10-08	04:00:00	177	40.42
2	ON	2003-10-10	12:20:00	177	
	OFF	2003-10-10	13:15:00	177	0.92
2	ON	2003-10-15	06:45:00	178	
	OFF	2003-10-15	08:20:00	178	1.58
2	ON	2003-10-20	01:00:00	179	
	OFF	2003-10-20	01:31:00	179	0.52
2	ON	2003-10-20	03:01:00	179	
	OFF	2003-10-22	11:20:00	179	56.32
2	ON	2003-10-24	18:55:00	179	
	OFF	2003-10-24	20:45:00	180	1.83
2	ON	2003-10-27	04:15:00	180	
	OFF	2003-10-27	05:50:00	180	1.58
2	ON	2003-10-29	12:50:00	180	
	OFF	2003-10-31	22:20:00	180	57.50
2	ON	2003-11-03	07:15:00	181	
	OFF	2003-11-04	12:18:00	181	29.05
2	ON	2003-11-04	13:48:00	181	
	OFF	2003-11-05	16:10:00	181	26.37
2	ON	2003-11-08	01:40:00	181	
	OFF	2003-11-08	03:20:00	182	1.67
2	ON	2003-11-10	10:15:00	182	
	OFF	2003-11-10	11:50:00	182	1.58
2	ON	2003-11-12	21:25:00	182	
	OFF	2003-11-15	06:20:00	183	56.92
2	ON	2003-11-19	23:00:00	183	
	OFF	2003-11-20	00:40:00	183	1.67
2	ON	2003-11-22	07:45:00	183	
	OFF	2003-11-24	18:01:00	184	58.27
2	ON	2003-11-27	02:05:00	184	
	OFF	2003-11-27	03:45:00	184	1.67
2	ON	2003-11-29	10:45:00	184	
	OFF	2003-11-29	12:20:00	185	1.58
2	ON	2003-12-01	20:15:00	185	
	OFF	2003-12-04	06:45:00	185	58.50
2	ON	2003-12-08	23:30:00	186	
	OFF	2003-12-09	00:40:00	186	1.17
2	ON	2003-12-11	08:10:00	186	
	OFF	2003-12-11	20:55:00	186	12.75
2	ON	2003-12-11	23:55:00	186	
	OFF	2003-12-13	17:30:00	186	41.58
2	ON	2003-12-16	02:35:00	187	
	OFF	2003-12-16	03:53:00	187	1.30

continued…

SC		Day	Time	Planning Period	Duration (hours)
2	ON	2003-12-20	22:30:00	188	
	OFF	2003-12-23	07:10:00	188	56.67
2	ON	2003-12-28	00:00:00	188	
	OFF	2003-12-28	01:10:00	189	1.17
2	ON	2003-12-30	08:40:00	189	
	OFF	2003-12-30	18:35:00	189	9.92
2	ON	2003-12-30	21:35:00	189	
	OFF	2004-01-01	18:10:00	189	44.58
2	ON	2004-01-04	03:05:00	189	
	OFF	2004-01-04	04:40:00	190	1.58
2	ON	2004-01-08	21:25:00	190	
	OFF	2004-01-09	02:20:00	190	4.92
2	ON	2004-01-09	05:20:00	190	
	OFF	2004-01-10	05:14:00	190	23.90
2	ON	2004-01-10	08:14:00	190	
	OFF	2004-01-11	07:40:00	191	23.43
2	ON	2004-01-16	00:35:00	191	
	OFF	2004-01-16	00:40:00	191	0.08
2	ON	2004-01-18	11:00:00	192	
	OFF	2004-01-18	17:40:00	192	6.67
2	ON	2004-01-18	20:40:00	192	
	OFF	2004-01-20	18:45:00	192	46.08
2	ON	2004-01-23	03:35:00	192	
	OFF	2004-01-23	05:05:00	192	1.50
2	ON	2004-01-25	12:40:00	192	
	OFF	2004-01-25	14:30:00	193	1.83
2	ON	2004-01-27	22:05:00	193	
	OFF	2004-01-30	08:20:00	193	58.25
2	ON	2004-02-01	16:10:00	193	
	OFF	2004-02-01	17:19:00	193	1.15
2	ON	2004-02-01	17:20:00	194	
	OFF	2004-02-01	17:56:00	194	0.60
2	ON	2004-02-04	01:05:00	194	
	OFF	2004-02-04	02:18:00	194	1.22
2	ON	2004-02-04	02:19:00	194	
	OFF	2004-02-04	02:41:00	194	0.37
2	ON	2004-02-06	12:23:00	194	
	OFF	2004-02-08	20:35:00	194	56.20
2	ON	2004-02-08	20:36:00	195	
	OFF	2004-02-08	21:11:00	195	0.58
2	ON	2004-02-11	04:10:00	195	
	OFF	2004-02-11	05:37:00	195	1.45
2	ON	2004-02-11	05:38:00	195	
	OFF	2004-02-11	05:46:00	195	0.13

continued…

SC		Day	Time	Planning Period	Duration (hours)
2	ON	2004-02-15	22:40:00	196	
	OFF	2004-02-18	07:20:00	196	56.67
2	ON	2004-02-23	01:45:00	197	
	OFF	2004-02-23	03:20:00	197	1.58
2	ON	2004-02-25	12:40:00	197	
	OFF	2004-02-27	21:45:00	198	57.08
2	ON	2004-03-01	04:50:00	198	
	OFF	2004-03-01	06:30:00	198	1.67
2	ON	2004-03-03	15:27:00	198	
	OFF	2004-03-03	16:05:00	198	0.63
2	ON	2004-03-05	23:15:00	198	
	OFF	2004-03-06	00:43:00	199	1.47
2	ON	2004-03-06	02:13:00	199	
	OFF	2004-03-08	10:34:00	199	56.35
2	ON	2004-03-10	17:57:00	199	
	OFF	2004-03-10	19:20:00	199	1.38
2	ON	2004-03-13	02:20:00	199	
	OFF	2004-03-13	03:55:00	200	1.58
2	ON	2004-03-15	12:56:00	200	
	OFF	2004-03-17	22:25:00	200	57.48
2	ON	2004-03-20	05:35:00	200	
	OFF	2004-03-20	07:47:00	201	2.20
2	ON	2004-03-24	23:55:00	201	
	OFF	2004-03-25	05:30:00	201	5.58
2	ON	2004-03-25	08:30:00	201	
	OFF	2004-03-27	09:00:00	201	48.50
2	ON	2004-03-29	18:20:00	202	
	OFF	2004-03-29	19:55:00	202	1.58
2	ON	2004-04-01	03:00:00	202	
	OFF	2004-04-01	04:40:00	202	1.67
2	ON	2004-04-03	12:30:00	202	
	OFF	2004-04-03	13:52:00	203	1.37
2	ON	2004-04-03	15:22:00	203	
	OFF	2004-04-05	23:00:00	203	55.63
2	ON	2004-04-08	08:11:00	203	
	OFF	2004-04-08	12:05:00	203	3.90
2	ON	2004-04-08	15:05:00	203	
	OFF	2004-04-10	17:25:00	204	50.33
2	ON	2004-04-13	00:25:00	204	
	OFF	2004-04-13	07:20:00	204	6.92
2	ON	2004-04-13	10:20:00	204	
	OFF	2004-04-15	09:50:00	204	47.50
2	ON	2004-04-17	18:55:00	204	
	OFF	2004-04-18	06:10:00	205	11.25

continued…

Doc. No.   CAA-EST-UG-RAP
Issue: 7.1
Date: 2025-03-01

Project: Cluster Science Archive   Page: 43 of 48

SC		Day	Time	Planning Period	Duration (hours)
2	ON	2004-04-18	09:10:00	205	
	OFF	2004-04-20	03:40:00	205	42.50
2	ON	2004-04-22	14:50:00	205	
	OFF	2004-04-24	23:30:00	206	56.67
2	ON	2004-04-27	08:50:00	206	
	OFF	2004-04-29	17:43:00	206	56.88
2	ON	2004-05-02	01:00:00	206	
	OFF	2004-05-02	02:19:00	206	1.32
2	ON	2004-05-02	13:31:00	207	
	OFF	2004-05-02	14:04:00	207	0.55
2	ON	2004-05-02	20:00:00	207	
	OFF	2004-05-04	08:50:00	207	36.83
2	ON	2004-05-06	13:55:00	207	
	OFF	2004-05-06	20:10:00	207	6.25
2	ON	2004-05-07	00:10:00	207	
	OFF	2004-05-08	21:50:00	208	45.67
2	ON	2004-05-11	13:03:00	208	
	OFF	2004-05-12	04:18:00	208	15.25
2	ON	2004-05-12	06:18:00	208	
	OFF	2004-05-13	11:45:00	208	29.45
2	ON	2004-05-15	17:50:00	208	
	OFF	2004-05-16	02:17:00	209	8.45
2	ON	2004-05-16	03:53:00	209	
	OFF	2004-05-18	04:20:00	209	48.45
2	ON	2004-05-20	12:36:00	209	
	OFF	2004-05-20	18:51:00	209	6.25
2	ON	2004-05-20	23:39:00	209	
	OFF	2004-05-22	22:20:00	210	46.68
2	ON	2004-05-25	06:00:00	210	
	OFF	2004-05-25	14:30:00	210	8.50
2	ON	2004-05-25	16:30:00	210	
	OFF	2004-05-27	14:03:00	210	45.55
2	ON	2004-05-29	23:50:00	210	
	OFF	2004-05-30	01:28:00	211	1.63

From Planing Periods 567–568, SC2 and SC3
Special operations as part of Guest Investigator Program 2011

SC		Day	Time	Planning Period	Duration (hours)
2	ON	2011-03-29	10:03:00	567	
	OFF	2011-03-29	15:03:00	567	5.00
2	ON	2011-03-31	16:07:00	567	
	OFF	2011-03-31	20:07:00	567	4.00
3	ON	2011-03-29	11:40:00	567	
	OFF	2011-03-29	16:40:00	567	5.00
3	ON	2011-03-31	17:09:00	567	
	OFF	2011-03-31	22:39:00	567	5.50
2	ON	2011-04-02	22:06:00	568	
	OFF	2011-04-03	03:06:00	568	5.00
3	ON	2011-04-02	22:44:00	568	
	OFF	2011-04-03	04:44:00	568	6.00

G List of Important Events for RAPID

(Updated to 2024 Sep 30)

Flags Legend

☞	Just a note	↗	IIMS high voltages increasing
✔	Something good happening	↘	IIMS high voltages decreasing
✖	Something bad happening	▼	Something dies
✪	IIMS Donut activity	¶	DPU programming changes

	S/C	Date	Time	Event
☞	❶❷❸❹	2000-12-07	07:08	First time all 4 spacecraft turned on simultaneously.
☞	❶○○○	2000-12-07	—	Initial IIMS voltage levels = 4/5 (Start/Stop)
☞	○❷○○	2000-12-07	—	Initial IIMS voltage levels = 7/7
☞	○○❸○	2000-12-07	—	Initial IIMS voltage levels = 4/4
☞	○○○❹	2000-12-07	—	Initial IIMS voltage levels = 5/5
✔	❶❷❸❹	2001-02-01	—	Official start of operations.
¶	○○❸○	2001-04-26	15:07	Major post-commissioning patch
¶	○○○❹	2001-05-18	07:52	Major post-commissioning patch
¶	❶○○○	2001-05-18	09:30	Major post-commissioning patch
¶	○❷○○	2001-05-18	13:04	Major post-commissioning patch
✪↗	❶○○○	2001-08-18	00:00	Increase HV on SC1 to 6/7, because of donut
✪↗	○○❸○	2001-08-18	00:00	Increase HV on SC3 to 6/6, because of donut
✪↗	○○○❹	2001-08-18	00:00	Increase HV on SC4 to 7/7, because of donut
✪↗	○❷○○	2001-10-14	23:47	Increase HV on SC2 to 8/8, because of donut
✪↗	❶○○○	2001-11-01	09:00	Increase HV on SC1 to 7/8, because of donut
✪↗	○○❸○	2001-11-01	09:00	Increase HV on SC3 to 7/7, because of donut
✪↗	○○○❹	2001-11-01	09:00	Increase HV on SC4 to 8/8, because of donut
✪↗	○❷○○	2001-12-01	23:52	Increase HV on SC2 to 9/9, because of donut
↗	○○❸○	2002-04-08	00:00	Increase HV on SC3 to 8/8
☞	○○❸○	2002-07-23	07:24:00	IES channels, Ver. 3 Autoswitching Ver. 2, revised parameters
☞	○❷○○	2002-07-23	08:28:00	IES channels, Ver. 3 Autoswitching Ver. 2
☞	❶○○○	2002-07-25	08:15:00	IES channels, Ver. 3 Autoswitching Ver. 2
☞	○○○❹	2002-07-30	07:16:42	IES channels, Ver. 3 Autoswitching Ver. 2
✖	○○○❹	2003-06-21	17:15	Only ion head 1 functioning on SC4 (until May 2006)
✔	○❷○○	2003-07-26	09:50	Start of first NM3 interval on SC2 Equivalent to BM for RAPID, done every 6th (later 4th) orbit, until May, 2004
↗	❶○○○	2003-08-24	11:11	Increase HV on SC1 to 8/9
↗	○❷○○	2003-08-24	11:11	Increase HV on SC2 to 10/10
↗	○○❸○	2003-08-24	11:11	Increase HV on SC3 to 9/9

continued...

. . . RAPID events continued

	S/C	Date	Time	Event
↗	○○○❹	2003-08-24	11:11	Increase HV on SC4 to 9/9
✔♬	❶○○○	2004-04-20	10:00	Start of L3DD on SC1.
✔♬	○○❸○	2004-04-30	07:19	Start of L3DD on SC3.
✔♬	○○○❹	2004-05-03	11:19	Start of L3DD on SC4.
✔♬	○❷○○	2004-05-13	15:38	Start of L3DD on SC2.
✖	○❷○○	2004-05-30	01:28	End of last NM3 interval on SC2 (Has been replaced by L3DD on all SC)
↗	❶○○○	2004-11-15	01:30	Increase HV on SC1 to 9/10
↗	○❷○○	2004-11-15	01:30	Increase HV on SC2 to 11/11
↗	○○❸○	2004-11-15	01:30	Increase HV on SC3 to 10/10
↗	○○○❹	2004-11-15	01:30	Increase HV on SC4 to 10/10
✔	○○❸○	2005-10-06	—	SAA range on SC3 set to 94.6°–97.6°, to reduce solar noise in electron head 1 (other SC are 93.2°–96.2°) (Critical SAA values are ~96° and <94.6°)
✔	○○○❹	2006-05-09	13:27	SC4 recovers, ion heads 1 and 3 functioning once more (rebooted)
↗	❶○○○	2006-08-20	11:17	Increase HV on SC1 to 10/11
↗	○❷○○	2006-08-20	11:17	Increase HV on SC2 to 12/12
↗	○○❸○	2006-08-20	11:17	Increase HV on SC3 to 11/11
↗	○○○❹	2006-08-20	11:17	Increase HV on SC4 to 11/11
☞	○○❸○	2006-08-28	12:46:00	IES channels, Ver. 4, values standardized as much as possible
☞	○○○❹	2006-09-19	15:03:00	IES channels, Ver. 4
☞	❶○○○	2006-09-21	11:30:00	IES channels, Ver. 4
☞	○❷○○	2006-09-21	13:33:00	IES channels, Ver. 4
↗	❶○○○	2007-03-03	04:19	Increase HV on SC1 to 11/12
↗	○❷○○	2007-03-03	04:19	Increase HV on SC2 to 13/13
↗	○○❸○	2007-03-03	04:19	Increase HV on SC3 to 12/12
↗	○○○❹	2007-03-03	04:19	Increase HV on SC4 to 12/12
▼	❶○○○	2007-03-16	06:00	End of ions on SC1.
↘	○❷○○	2007-03-31	21:23	Decrease HV on SC2 to 12/12
↗	○❷○○	2007-05-06	14:39	Restore HV on SC2 to 13/13
✖	○○❸○	2008-01-28	23:38	Only ion head 1 functioning on SC3
✔	○○❸○	2008-03-18	15:06	SC3 recovers, ion heads 1 and 3 functioning again (rebooted)
↗	○❷○○	2008-03-29	17:32	Increase HV on SC2 to 14/14
↗	○○❸○	2008-03-30	01:01	Increase HV on SC3 to 13/13
↗	○○○❹	2008-03-30	01:01	Increase HV on SC4 to 13/13
☞	○○❸○	2008-04-25	—	Start 45° tilt compaign on SC3
☞	○○❸○	2008-05-30	—	End 45° tilt compaign on SC3
▼	○○❸○	2009-12-01	—	End of ions on SC3
☞	❶❷❸❹	2010-07-05	—	Start turning down HV in radiation belts

. . . RAPID events continued

	S/C	Date	Time	Event
↗	○○○❹	2010-10-22	20:40	Increase HV on SC4 to 14/14
✖	○❷○❹	2011-08-14	20:00	Only ion head 1 functioning on SC2 and SC4
✔	○❷○○	2011-09-12	15:17	SC2 recovers, ion heads 1 and 3 functioning again (rebooted)
✔	○○○❹	2011-09-14	12:00	SC4 recovers, ion heads 1 and 3 functioning again (rebooted)
☞	○❷○○	2011-10-28	14:14:28	IES channels, Ver. 5
☞	○○○❹	2011-10-28	16:00:58	IES channels, Ver. 5
☞	❶○○○	2011-11-01	08:25:38	IES channels, Ver. 5
☞	○○❸○	2011-11-01	16:48:38	IES channels, Ver. 5
✖	○❷○○	2012-01-13	—	Ion head 1 on SC2 stops working
✔	○❷○○	2012-05-31	—	Ion head 1 on SC2 recovers
✖	○❷○○	2012-10-15	—	Ion head 1 on SC2 stops working
↗	○❷○○	2013-03-08	23:30	Increase HV on SC2 to 15/15, max value
✔	○❷○○	2013-03-08	23:30	Ion head 1 on SC2 recovers
☞	❶○○○	2013-11-05	16:58:10	IES channels, Ver. 6 / Autoswitching Ver. 3 (faster switch to lower times)
☞	○○○❹	2013-11-06	14:49:27	IES channels, Ver. 6 / Autoswitching Ver. 3
☞	○○❸○	2013-11-06	18:23:02	IES channels, Ver. 6 / Autoswitching Ver. 3
☞	○❷○○	2013-11-06	19:22:57	IES channels, Ver. 6 / Autoswitching Ver. 3
☞	❶○○○	2014-03-13	12:26:00	IES channels, Ver. 7
✖	○○❸○	2014-05-01	—	SAA on SC3 crosses critical 94.6° limit; high solar contamination in electron detectors 1–3 in all channels; will be permanent condition
☞	❶❷❸❹	2014-05-19	—	Spin axis fixed on all SC; SAA will range 87.6°–92.4° over one year; currently 88.2° on all, including SC3 with solar contamination
▼	○❷○○	2015-03-26	07:00	Partial failure of electrons on SC2
✖	○❷○○	2015-06-20	21:50	Ion head 1 on SC2 becomes very insensitive
✔	○❷○○	2015-06-12	—	Recover electron head 3 on SC2, with caveats, ie, autoswitching not working reliably, spikes need suppressing, geometry factors need correcting
☞	❶○○○	2016-05-09	20:23:48	IES channels, Ver. 8
☞	○❷○○	2016-05-09	09:14:56	IES channels, Ver. 8
☞	○○❸○	2016-05-09	09:09:04	IES channels, Ver. 8
☞	○○○❹	2016-05-09	20:59:31	IES channels, Ver. 8
☞	○○❸○	2016-05-20	04:35	Autoswitching Ver. 4
☞	○○○❹	2016-05-20	04:28	Autoswitching Ver. 4
☞	❶○○○	2016-05-21	00:53	Autoswitching Ver. 4
☞	○❷○○	2016-05-25	10:12	Autoswitching Ver. 6
☞	❶❷❸❹	2017-03-01	—	IES channels, Ver. 9 (effective after eclipse season)

continued. . .

Doc. No.   CAA-EST-UG-RAP
Issue: 7.1
Date: 2025-03-01

Project: Cluster Science Archive   Page: 48 of 48

. . . RAPID events continued

	S/C	Date	Time	Event
↗	○○○❹	2017-12-04	04:00	Increase HV on SC4 to 15/15, max value
✖	○❷○○	2017-12-21	—	Ion head 1 on SC2 effectively dead
☞	○○○❹	2018-02-06	—	IES channels, Ver. 10
☞	❶○○○	2018-02-07	—	IES channels, Ver. 10
☞	○❷❸○	2018-02-08	—	IES channels, Ver. 10
✔	○❷○○	2018-09-08	—	Ion head 1 on SC2 recovers
☞	○❷○○	2018-09-17	18:55	IES channels, Ver. 11
☞	○○○❹	2018-09-17	18:58	IES channels, Ver. 11
☞	❶○○○	2018-09-18	10:20	IES channels, Ver. 11
☞	○○❸○	2018-09-18	18:05	IES channels, Ver. 11
☞	❶❷❸❹	2019-09-12	—	IES channels, Ver. 12
✖	❶❷❸❹	2020-03-20	—	Power down because of COVID-19 crisis at ESOC
✔	❶❷❸❹	2020-04-07	—	End of COVID-19 pause
☞	❶❷❸❹	2020-09-12	—	IES channels, Ver. 13
☞	○○❸○	2020-10-21	11:21	IES channels, Ver. 14
☞	❶○○○	2020-10-21	12:20	IES channels, Ver. 14
☞	○○○❹	2020-10-21	12:32	IES channels, Ver. 14
☞	○❷○○	2020-10-23	18:48	IES channels, Ver. 14
☞	❶❷❸❹	2021-09-12	—	IES channels, Ver. 15
☞	❶❷❸❹	2022-03-15	—	IES channels, Ver. 16
☞	○○❸○	2023-05-25	14:19	IES channels, Ver. 17
☞	❶○○○	2023-05-30	08:59	IES channels, Ver. 17
☞	○❷○○	2023-06-01	07:29	IES channels, Ver. 17
☞	○○○❹	2023-06-01	13:49	IES channels, Ver. 17
☞	○○❸○	2023-06-30	13:51	IES channels, Ver. 17b
✖	❶○○○	2023-09-19	00:00	RAPID on SC1 permanently turned off
✖	○❷○○	2024-02-01	03:58	Payloads on SC2 permanently turned off
☞	○○○❹	2024-04-30	12:49	IES channels, Ver. 17b
☞	○○❸○	2024-08-22	09:11	IES channels, Ver. 18
☞	○○○❹	2024-08-22	06:12	IES channels, Ver. 18
✖	○○❸❹	2024-10-01	00:00	Payloads on SC3 and SC4 permanently turned off **End Of Operations**